UNIVERSITY OF WARMIA AND MAZURY IN OLSZTYN

Technical Sciences

17(4) 2014

PUBLISHER UWM

OLSZTYN 2014

The Technical Sciences is indexed and abstracted in BazTech (http://baztech.icm.edu.pl) and in IC Journal Master List (http://journals.indexcopernicus.com)

The Journal is also available in electronic form on the web sites
http://www.uwm.edu.pl/techsci (subpage Issues)
http://wydawnictwo.uwm.edu.pl (subpage Czytelnia)

The print edition is the primary version of the Journal

PL ISSN 1505-4675

Address
ul. Jana Heweliusza 14
10-718 Olsztyn-Kortowo, Poland
tel.: +48 89 523 36 61
fax: +48 89 523 34 38
e-mail: wydawca@uwm.edu.pl

Ark. wyd. 7,1, ark. druk. 5,75, nakład 95 egz.
Druk – Zakład Poligraficzny UWM w Olsztynie
zam. nr 53

Contents

Technical Sciences 17(4), 2014, 315–320

CREEP OF CONCRETE – THE SHORT STUDY CONDUCTED AT THE NEW LABORATORY AT THE UNIVERSITY OF WARMIA AND MAZURY IN OLSZTYN

Dawid Pawliszyn, Krzysztof Klempka

The Chair of Mechanics and Building Structures
University of Warmia and Mazury in Olsztyn

Received 10 March 2014, accepted 9 November 2014, available on line 12 November 2014

K e y w o r d s: concrete, creep of concrete, compression, shrinkage, creep coefficient.

A b s t r a c t

In order to launch the newly bought creep testing machine, concrete creep was studied. The creep coefficients were calculated and the results were compared to results reached based on Eurocode 2 regulations. The results were compatible.

Introduction

The phenomenon of creep is the tendency of a solid material to deform permanently under the influence of load over a period of time. Creep must be taken into account in the design of prestressed concrete structures and significantly influences internal forces in RC elements in compression as well as deflections resulting from bending. It also influences to a lesser degree (which is nonetheless present in the codes) the width of cracks. In prestressed structures, creep and shrinkage lead to a loss of prestressing force. Creep increases deflections of slender beams. In columns creep decreases concrete stresses but increases reinforcement stresses. Reinforcement with time takes over the part of load that was initially carried by concrete. This is why in order to study the reinforced concrete structures influenced by long term loads it is necessary to be able to calculate the creep of concrete.

The newly opened UWM laboratory for technical control of structures, built within the framework of the Regional Operational Programme Warmia

Correspondence: Krzysztof Klempka, Katedra Mechaniki i Konstrukcji Budowlanych, Uniwersytet Warmińsko-Mazurski, ul. Heweliusza 4, 10-724 Olsztyn, e-mail: kik@uwm.edu.pl

and Mazury for the years 2007–2013, has been equipped with creep testing machine (Fig. 1) Type HKB-1000 kN (and its software), which has been placed in an air-conditioned chamber.

Fig. 1. Concrete creep testing machine Type HKB-1000 kN manufactured by walter+bai ag

Creep Testing Machine Series HKB specially designed for long term creep tests on concrete specimens up to ϕ 160 or cubes 150 mm by means of a pressure exerted load. Tests can be carried out either on a single sample or on several specimens in series. The load cylinder is put under pressure by a hand pump. The force can be read of the pressure gauge or electric read out and is kept constant by a compressed gas storage system. Main technical data: max. compression force 1000 kN, machine grad (from 100 to 1000 kN) – Grade 1, max. distance between compression platen 1250 mm, min. distance 290 mm, piston stroke 20 mm, lower and upper compression platen ϕ 200 mm. The launch process of the new equipment involved the study described later in the paper.

Creep study

The study of creep was carried out using cylinder specimens d = 150 mm and the height h = 300 mm, according to ITB instructions, number 194 and the fast-setting cement CEM II/A-V 42,5 R. The specimens after twenty-four hours were placed in an air-conditioned chamber at the temperature of 20°C and relative humidity over 90% for seven days. Next, the specimens were

placed in an air-conditioned chamber with 50% relative humidity and a temperature of 20°C and stored there until the time of the experiment. Since it is necessary to decrease the deformations resulting from creep by shrinkage, another load-free specimen was prepared to measure shrinkage. All the specimens prepared for measuring creep and other accompanying parameters were stored in the same conditions. An extensometer was used with the resolution of 1/100 mm and the measuring base of 250 mm (Fig. 2) The benchmarks were installed alongside three lines evenly placed on the side of the cylinder (every 120 degrees). The analysis started at an concrete age of 14 days. First, the compressive strength of concrete was determined ($f_c(14)$ = 30,5 MPa), whose value became the base for calculating the level of long-term loads in the study of creep. After placing the sample in the creep testing machine, it was left without any load for an hour. Then, the initial measurement was taken, then the sample was loaded. The load was continually increased until the stress reached $\sigma = 0{,}4f_c$ (the measurements were also taken at the levels of $0{,}5\sigma$, $2/3\sigma$, σ). The full load was reached within ten minutes.

The first measurement was taken after 5 minutes, and the result was defined as temporary deflection. The next measurements were taken for 253 days, in the first week every day, during the next three months, once a week, and then only once a month.

The creep measurements were accompanied by shrinkage measurements. The load-free sample was placed in the same position and the same air-conditioned chamber as the loaded sample. Based on the results, the creep curve was determined (Fig. 3).

Fig. 2. Deformation measurement with the use of the extensometer

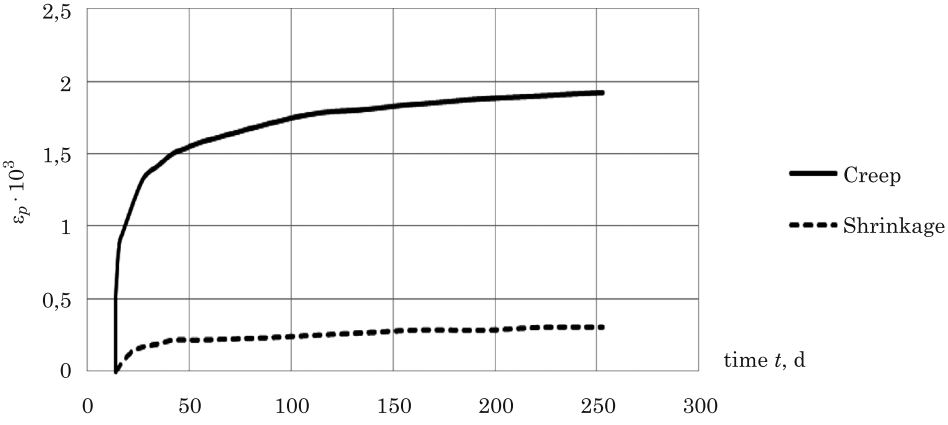

Fig. 3. Creep curve for axial compression (t_0 = 14d, $f_c(14)$ = 30,5 MPa), the stress equals 0,4$f_c(14)$

Comparison of experimental creep coefficients with values calculated according Eurocode 2

Later in the paper, the coefficients obtained in the study and by following Eurocode 2 regulations were compared. The values of coefficients in the study were obtained from the following relation:

$$\varphi(t,t_0) = \frac{\varepsilon_p(t,t_0)}{\varepsilon_d(t_0)} = \frac{\varepsilon_c(t,t_0) - \varepsilon_{cs}(t,t_0) - \varepsilon_d(t_0)}{\varepsilon_d(t_0)} \tag{1}$$

where:
$\varepsilon_p(t,t_0)$ – is creep strain after t time of the specimen loaded in t_0 time,
$\varepsilon_c(t,t_0)$ – is total strain in t time,
$\varepsilon_{cs}(t,t_0)$ – shrinkage in t time,
$\varepsilon_d(t_0)$ – is instantaneous strain after 5 minutes of loading.

According to Eurocode 2 creep coefficients can be obtained from the formula:

$$\varphi(t,t_0) = \varphi_0\beta_c(t,t_0) \tag{2}$$

where:
φ_0 – the basic creep coefficient, and function $\beta_c(t,t_0)$ shows the progress of creep in time depending on $(t - t_0)$, (RH), h_0 and f_{cm}.

These values were obtained based on Eurocode 2, Annex B. For calculations it was assumed that the relative humidity was RH = 50%, the notional size of

the cross section was h_0 = 75 mm and the average strength of concrete aged 28 days was f_{cm} = 34,33 MPa. An adjusted age of concrete was taken into account and was defined by coefficient α = 1 for class R cement. The results were presented in Table 1. In bold are the values of creep coefficients obtained through the study. They are higher than the ones obtained according to Eurocode 2.

Table 1

Comparison of experimental creep coefficients and coefficients according to Eurocode 2

t_0 [d]	t [d]	$\varphi_1 = \varphi(t,t_0)$ according to the study	$\varphi_2 = \varphi(t,t_0)$ according to Eurocode 2	$\frac{\lvert\varphi_2 - \varphi_1\rvert}{\varphi_1} 100\%$
14	15	0.47	0.56	19.15
	16	0.68	0.69	1.47
	17	0.72	0.78	8.33
	18	0.76	0.85	11.84
	19	0.81	0.91	12.34
	20	0.85	0.96	12.94
	21	0.91	1.00	9.89
	22	0.95	1.04	9.47
	23	1.05	1.08	2.86
	28	**1.29**	1.23	4.65
	35	**1.41**	1.38	2.12
	42	**1.52**	1.50	1.31
	49	1.59	1.59	0.00
	56	1.67	1.67	0.00
	105	1.97	2.03	3.04
	133	2.01	2.17	7.96
	161	2.05	2.27	10.73
	197	2.13	2.37	11.27
	225	2.14	2.44	14.02
	253	2.16	2.50	15.74

Conclusions

The new creep testing machine was put to use. For elements loaded in the age of fourteen days to a stress of $0{,}4f_c(t_0)$ coefficients of concrete creep were determined after t time in which measurements were taken. The results of the study were compared with the results calculated according to Eurocode 2. They were fairly compatible. The differences between the results are not greater than 20%. For the most part of the analysis, the values obtained through

calculations turned out to be greater than the ones obtained experimentally. In opposite cases, the differences are insignificant.

References

PN-EN 1992-1-1: 2004. Eurokod 2. *Projektowanie konstrukcji z betonu*. Część 1–1: *Reguły ogólne i reguły dla budynków*.

Instrukcja ITB nr 194. 1998. *Badania cech mechanicznych betonu na próbkach wykonanych w formach*. Wyd ITB, Warszawa.

KNAUFF M. 2012. *Obliczanie konstrukcji żelbetowych według Eurokodu 2*. Wyd Naukowe PWN, Warszawa.

MITZEL A. 1972. *Reologia betonu*. Arkady, Warszawa.

NAGRODZKA-GODYCKA K. 1999. *Badanie właściwości betonu i żelbetu w warunkach laboratoryjnych*. Arkady, Warszawa.

NEVILLE A.M., DILGER W.H., BROOKS J.J. 1983. *Creep of plain and structural concrete*. Construction Press, London and New York.

ULICKII I.I. 1967. *Teoria i rasczot żeliezobietonnych stierzniewych konstrukcji s uczotom dlitielnnych prociesow*. Izdatielstwo Budiwielnik, Kijew.

Technical Sciences 17(4), 2014, 321–335

DARCY'S AND FORCHHEIMER'S LAWS IN PRACTICE. PART 1. THE EXPERIMENT

***Wojciech Sobieski*[1], *Anna Trykozko*[2]**

[1] Department of Mechanics and Machine Design
University of Warmia and Mazury in Olsztyn
[2] Interdisciplinary Centre for Mathematical and Computational Modeling
University of Warsaw

Received 3 April 2014, accepted 8 November 2014, available on line 11 November 2014.

K e y w o r d s: Darcy's law, Forchheimer's law, Forchheimer Plot Method, porous media, permeability.

A b s t r a c t

The aim of this study is to derive flow parameters, which are permeability and Forchheimer coefficient, based on experimentally measured flow rates and pressure drops. When flow rates used in measurements exceed the limits of linear Darcy's flow regime we discuss what needs to be taken into account while processing the measurements. The study consists of two parts. In this part we briefly recall Darcy's and Forchheimer's laws and address the issue of detecting transition between ranges of their applicability. Then we describe the experiment and discuss 8 different ways to process measurement data, four for Darcy's, and four for Forchheimer's models. The main topic of the second part is to provide recommendations for the best ways to process data, so that the results obtained with numerical models are in the best agreement with the experimental data. The results shown in the two papers belong to a larger work devoted to modeling fluid flows through porous media, with a special interest in granular beds.

Introduction

A fundamental law linking pressure drop and velocity in fluid flow through porous media is Darcy's law (1856). It can be applied to flows of gases, liquids, or mixtures. Darcy's law may be written as follow (BEAR 1972, CATALANO 2012, HELLSTRÖM, LUNDSTRÖM 2006):

$$-\frac{\mathrm{d}p}{\mathrm{d}x} = \frac{1}{\kappa} \cdot (\mu \cdot \vec{v_f}) \tag{1}$$

Correspondence: Wojciech Sobieski, Katedra Mechaniki i Podstaw Konstrukcji Maszyn, Uniwersytet Warmińsko-Mazurski, ul. M. Oczapowskiego 11, 10-957 Olsztyn, phone: +48 89 523 32 40, e-mail: wojciech.sobieski@uwm.edu.pl

where:
p – pressure [Pa],
x – coordinate [m],
κ – permeability coefficient [m^2],
μ – dynamic viscosity coefficient of the fluid [kg/(m · s)],
$\vec{v}_f$ – filtration velocity [m/s].

For low flow velocities, Darcy's law correctly describes the flow in porous media (HELLSTRÖM, LUNDSTRÖM 2006). However, as velocities become larger, a discrepancy between experimental data and results obtained for Darcy's law appears. FORCHHEIMER (1901) linked this discrepancy to inertial effects and suggested to add to (1) a term representing kinetic energy (ANDRADE et al. 1999, BEAR 1972, EWING et al. 1999, HELLSTRÖM, LUNDSTRÖM 2006):

$$-\frac{\mathrm{d}p}{\mathrm{d}x} = \frac{1}{\kappa} \cdot (\mu \cdot \vec{v}_f) + \beta \cdot (\rho \cdot \vec{v}_f^{\,2}) \tag{2}$$

where:
β – Forchheimer coefficient (also known as non-Darcy coefficient, or β factor) [1/m],
ρ – density of the fluid [kg/m^3].

It is common to define limits of the Darcy's law validity by means of Reynolds number Re [-], defined as

$$\mathrm{Re} = \frac{\rho \cdot |\vec{v}_f| \cdot d}{\mu} \tag{3}$$

where:
d – the average particle diameter [m].

Most often it is assumed that the upper limit of the applicability of Darcy's law is between Re = 1 and Re = 10 (BEAR 1972, CHAPMAN 1981, HASSANIZADEH, GRAY 1987, SUKOP et al. 2013, TINDALL et al. 1988). Other works indicate the upper limit of Darcy's law as Re = 1 (ALABI 2011), Re = 2 (HASSANIZADEH, GRAY 1987), Re = 3 (HASSANIZADEH, GRAY 1987) or Re = 5 (HASSANIZADEH, GRAY 1987, SAWICKI et al. 2004). Some authors suggest that the upper limit goes above Re = 10 (CHAPMAN 1981, HASSANIZADEH, GRAY 1987). This ambiguity raises a question about which model is appropriate in cases where a range of velocities under consideration probably goes beyond the Darcy's flow regime. In the current work we address this question.

Both laws (1) and (2) are well known and can be found in many textbooks and papers. The available literature provides many general formulas to calculate permeability and Forchheimer coefficients based on such parameters of porous media as porosity or tortuosity (HUANG, AYOUB 2008), but the formulas are usually empirical and not universal. As we have shown in (SOBIESKI, TRYKOZKO 2001), different formulas computed with a fixed set of parameters can lead to totally different values of β coefficients, ranging even over several orders of magnitude.

The problem of assigning appropriate models and coefficients raises a question of a strategy to choose while processing experimental data. It is important for practical purposes of real systems design, as well as to create and verify mathematical models.

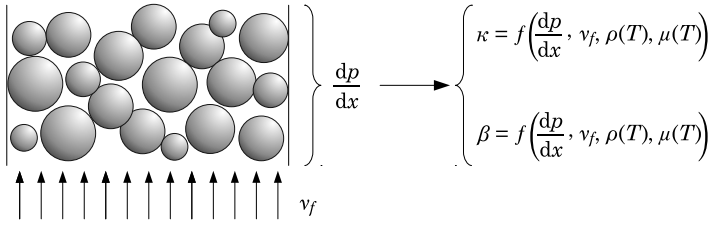

Fig. 1. The scheme of inverse problem

In the current work we suggest that in order to obtain all needed coefficients, an inverse problem using a test porous bed should be solved (Fig. 1). Thus obtained values may be used in other systems with the same porous medium and similar ranges of Reynolds numbers as well as in other investigations. Though the approach seems to be quite straightforward, there are several questions to be answered:

– How to prepare an experiment that will provide the best quality of results?

– In which way should the experimental data be analyzed?

– How to proceed in the case when the range of Reynolds numbers covered by the experiment spans over the Darcy's and Forchheimer flow regimes?

An attempt to discuss the above issues constitutes the main objectives of this study and is given mainly in the second part of the work. The current part contains details on preparing and collecting experimental data. The conclusions are based on the methodology developed in (SOBIESKI 2010), in which as the best experimental data we consider the data that gives the best agreement between numerical model (or the theory) and the experiment over the whole range of basic parameters.

It should be mentioned that a recent growth in available computer power has given rise to another approach, which we call a virtual experiment. Instead of a physical experiment, numerical simulations of flow at pore scale are performed by solving Navier-Stokes equations. Thanks to microimaging techniques it is feasible to consider flows in geometries reflecting realistic pore structures. By upscaling pore-scale solutions to the continuum core scale it is possible to study the models, parameters and appropriate relationships, see (PESZYŃSKA, TRYKOZKO 2013) and references therein.

Experimental study

A sketch of equipment used in experimental investigations is given in Figure 2. It consists of a plexiglass pipe filled with granulate (6), recharged from the bottom, with water coming from a container (1) through a pump (2). Intensity of flow is controlled by a valve (3). After passing through a bed, water reaches the upper reservoir (7), and then, through the overfall (8) goes down to the bottom reservoir. The flow intensity is measured by a rotameter (5). Piezometric heads

$$h = \frac{p}{\rho \cdot g} + z \tag{4}$$

where g is the gravity acceleration [m/s^2] and is a fixed reference level [m], are measured by means of U-tube manometers linked to connector pipes (10). Water temperature is measured by thermometer (9). Errors of measurement were as follows: flow intensity 0.000000056 [m^3/s]; piezometric head 1.0 [mm H_2O]; temperature 0.1 [K]. A glass bead pack was used as the porous medium. Main parameters are summarized in Tabela 1.

During the experiment, 10 measurements were made for each of 12 different values of volumetric flow Q^V. For a given volumetric flow, the resulting water levels (measured from a reference level) at four points along the measurement pipe were taken. The measurement points were equally distributed along the column with a distance 0.3 [m]. Based on these values and the column cross-section S, mean filtration velocity $\vec{v}_f$, pressure differences Δp between measurements points as well as Reynolds numbers were computed for every flow rate. In order to unify data and facilitate comparison with results of numerical simulation, pressures were related to the highest measurement point (Fig. 2, point 1). Results of measurements are summarized in Tabela 2.

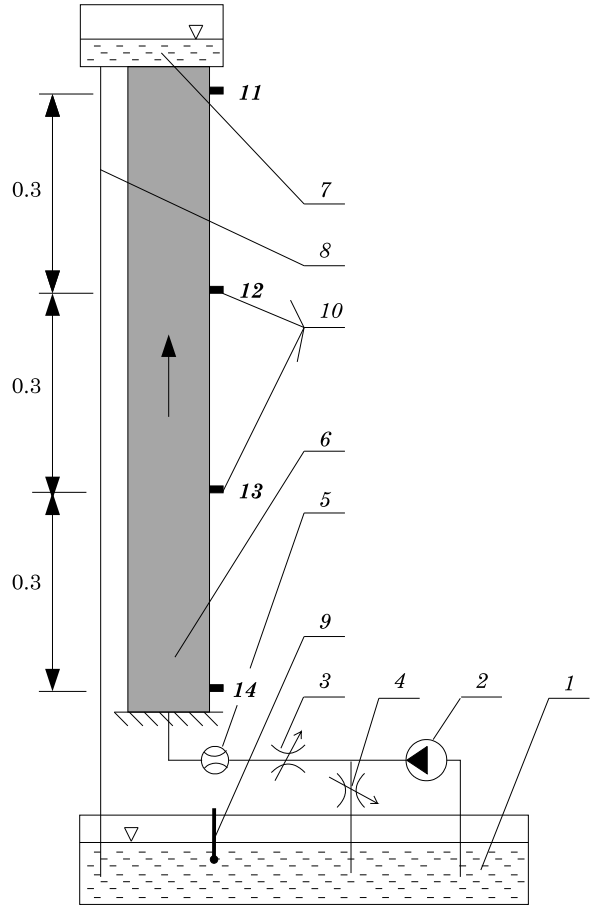

1 – bottom reservoir, *2* – pump, *3* – valve, *4* – overfall valve,
5 – rotameter, *6* – porous bed, *7* – upper reservoir,
8 – valve, *9* – thermometer, *10* – stub pipe,
11–14 – measurement points

Fig. 2. Scheme of the laboratory stand

A relationship between pressure drop and flow velocity imposed at the inlet is the basic relationship: its plot is given in Figure 3. Values obtained for pressure drop measured between extreme measurement points (thus, along the whole length of the column) are plotted with a solid line. Dashed lines mark minimum and maximum values of pressure drops measured for a given inlet velocity by applying different configurations of measurement sections. The relationship is non-linear, what suggests that the mesurements cover the region of the Fochheimer law's validity.

Increasing the length of the measurement section causes the global error of measurements to decrease. For this reason, in all computations that follow,

Table 1

Parameters of the experiment

Parameter	Symbol	Value
Average water temperature	T	306.63 [K]
Density of water	ρ	994.49 [kg/m^3]
Dynamic viscosity coefficient	μ	0.000742784 [kg/(m · s)]
Kinematic viscosity coefficient	ν	0.000000747 [m^2/s]
Area of a porous bed cross-section	S	0.005 [m^2]
Distance between measurement points 1–4	L	0.9 [m]
Porosity coefficient of granulate	e	0.37 [-]
Solid fraction	ε	0.63 [-]
Average diameter of glass beads	d	1.95 [mm]
Gravity acceleration	g	9.81 [m/s^2]

Table 2

Results of measurements

Q^V	h_1	h_2	h_3	h_4	$\vec{v}_f$	Δp_{4-1}	Δp_{3-1}	Δp_{2-1}	Re
$\cdot 10^{-3}$ [m^3/s]	[mm H_2O]	[mm H_2O]	[mm H_2O]	[mm H_2O]	$\cdot 10^{-3}$ [m/s]	[Pa]	[Pa]	[Pa]	[-]
5.66	357.50	362.20	365.90	370.60	0.313	127.80	81.95	45.85	0.82
22.09	**358.00**	**374.90**	**387.60**	**402.70**	**1.221**	**436.09**	**288.78**	**164.88**	**3.19**
38.52	**359.50**	**388.90**	**411.70**	**440.10**	**2.129**	**786.33**	**509.26**	**286.82**	**5.56**
54.95	**360.90**	**403.30**	**438.10**	**478.80**	**3.037**	**1150.22**	**753.16**	**413.65**	**7.93**
71.38	**362.80**	**419.20**	**466.60**	**520.50**	**3.945**	**1538.51**	**1012.67**	**550.23**	**10.30**
87.81	365.20	436.60	496.20	564.70	4.853	1946.31	1278.03	696.57	12.67
104.24	367.00	453.50	527.40	610.80	5.761	2378.50	1564.85	843.89	15.04
120.67	368.90	471.80	559.90	660.30	6.669	2842.88	1863.38	1003.89	17.41
137.11	371.40	492.10	598.00	716.50	7.577	3366.77	2210.70	1177.54	19.78
153.54	374.20	516.40	641.50	779.70	8.485	3956.03	2607.76	1387.29	22.15
169.97	376.60	541.80	685.70	845.70	9.393	4576.51	3015.56	1611.68	24.52
182.29	378.90	562.20	721.90	901.80	10.074	5101.38	3346.29	1788.26	26.30

pressure drops always refer to the longest section L. The pressure drop may be calculated directly between points 1 and 4, or indirectly, using an approximation method taking into account pressure drops between sections 3–1, 4–2, 3–2, 4–3 and 2–1 as well.

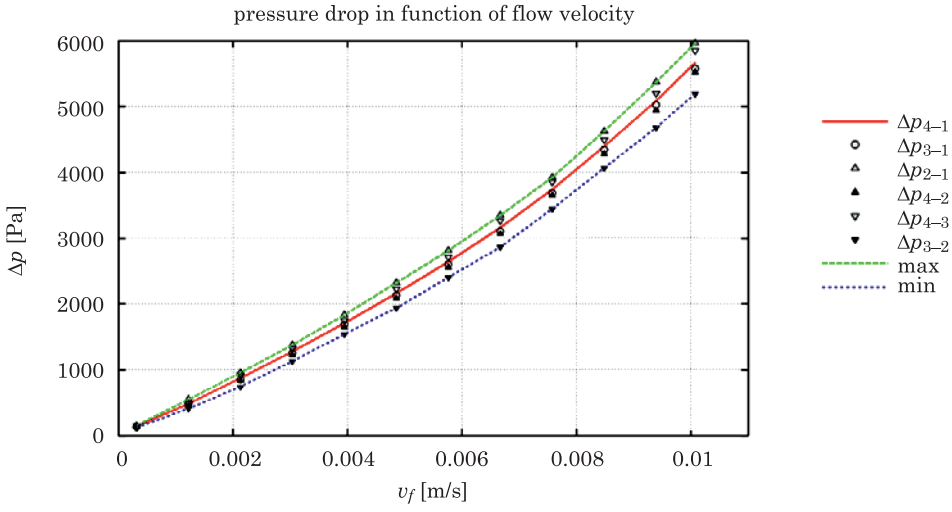

Fig. 3. Pressure drops measured between different pairs of measurement points

Figure 4 gives a plot of the effective permeability coefficient κ_{eff} as a function of velocity, computed following the formula:

$$\kappa_{eff} = \frac{\mu \cdot |\vec{v}_f|}{\frac{\mathrm{d}p}{\mathrm{d}x}} \tag{5}$$

A notion of 'effective' is used in order to emphasize that κ_{eff} in (5) is equivalent to the permeability coefficient κ in (1) only within the ranges of validity of Darcy's law. In general, coefficient κ_{eff} of (5) represents not only the permeability coefficient κ characterizing the medium, but also inertial effects. Effective permeability decreases with increasing flow velocities due to growing inertial effects. It is visible after rewriting the Forchheimer law (2) in the form:

$$-\frac{\mathrm{d}p}{\mathrm{d}x} = \left(\frac{1}{\kappa} + \frac{\beta \cdot \rho \cdot \vec{v}_f}{\mu}\right) \cdot \mu \cdot \vec{v}_f = \frac{\mu}{\kappa_{eff}} \cdot \vec{v}_f \tag{6}$$

It can be seen that the first point in Figure 4 differs from the others. The flow intensity in this case was very close to the lower limit of the measurement range of the rotameter. Since we doubt about reliability of this measurement, we decided not to take it into account in further investigations.

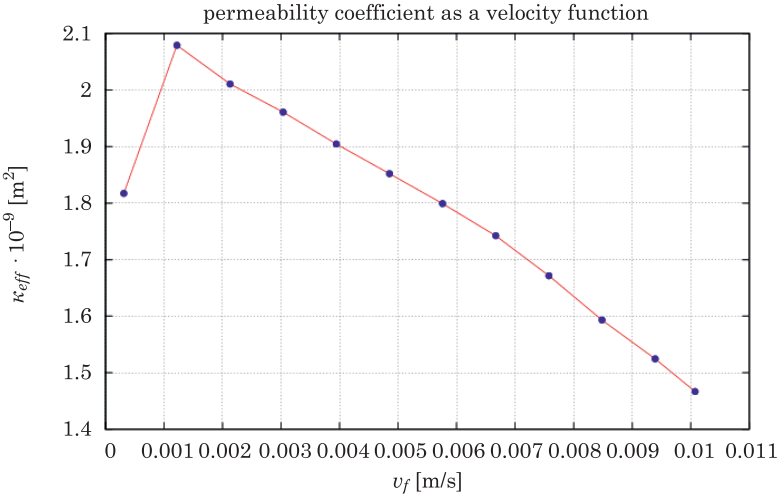

Fig. 4. Effective permeability coefficient as a function of velocity

Due to the rotameter characteristics we have not got enough data belonging to the linear flow regime what would be manifested by a constant ratio of flow rates and pressure drops. Thus the range of flow rates covered by the measurements does not allow to capture the onset of inertia effects. On the other hand, the Reynolds values less or close to 10 (Tab. 2) allow to consider flow cases 2–5 as belonging to the transition zone between the linear and nonlinear flow regimes. Therefore in what follows we consider the cases 2–5 as an approximation of the linear flow regime. Figure 5 shows the pressure drop calculated for the average value of the effective permeability coefficient according to Darcy's law. The averaging was performed two times: for cases 2–12 (the whole range of Reynolds numbers), and for flow cases 2–5. As expected, the linear model does not apply to the whole range of velocities. The discrepancy grows when the filtration velocities increase. This result shows why we consider the two cases: case 2–5 and case 2–12 separately.

After analyzing the measurement data and taking into account the range of Darcy's law validity we summarize that:

– The first point in Figure 4 will be not taken into account in further investigations due to the possibility of large flow measurement errors.

– All remaining values suggest presence of additional resistance forces in flow.

– We consider the flow case 5 as the last one to belong to the range of application of Darcy's law. The Reynolds number value for this measurement is close to the transition limit the most often suggested in the literature (Re $\approx$ 10). A distinction between the ranges of validity of Darcy's and

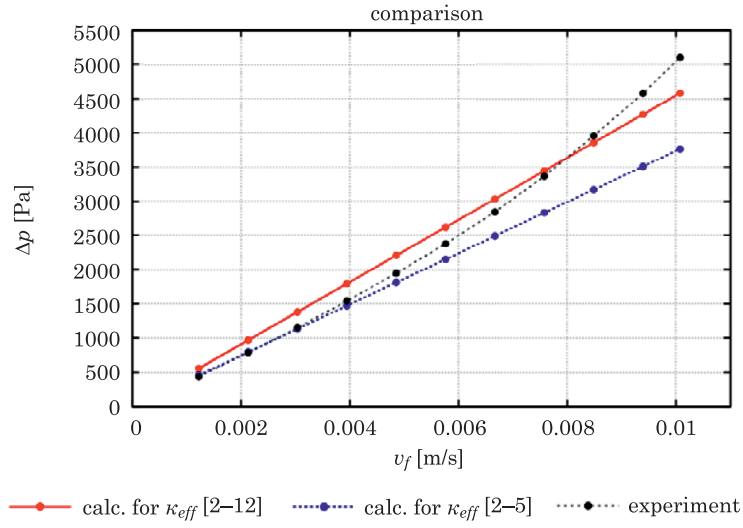

Fig. 5. Pressure drops as a function of velocity

Forchheimer's laws is necessary in order to perform further computations; this point will be discussed later.

– On the other hand, the transition between linear and non-linear regimes is smooth, therefore we are aware that this decision is somewhat arbitrary.

– The maximal Reynolds number reached during experiments does not exceed 30, and is thus several times smaller than the value considered to be the upper limit of validity of the Forchheimer law (HUANG, AYOUB 2008).

Computation of porous media parameter – linear model

The permeability coefficient κ is the main parameter characterizing porous media in a linear model. Four different methods were applied in order to compute this coefficient. Only results for measurements 2–5, with less or close to, were taken into account.

The first method followed directly Darcy's law (1) rewritten in the form:

$$\kappa = \mu \cdot \vec{v}_f \cdot \frac{L}{\Delta p} \tag{7}$$

where pressure drop along a segment $\Delta p/L$ replaces a more general notion of $\mathrm{d}p/\mathrm{d}x$.

Given measured piezometric heads h, differences Δp in pressures between the highest and the lowest measurement points were computed, to finally get the permeability coefficient κ. We also report values of the hydraulic conductivity coefficient K[m/s]

$$K = \kappa \cdot \frac{\rho \cdot g}{\mu} \tag{8}$$

which is commonly used in hydrogeology. As a last step, values of coefficients obtained for the same inlet velocities were averaged. Results are given in Table 3.

Table 3

Permeability coefficient calculations – method 1

$\vec{v_f} \cdot 10^{-3}$ [m/s]	Δh_{4-1} [m]	Δp_{4-1} [Pa/m]	K [m/s]	κ [m^2]
1.221	0.0447	484.545	0.02458	1.871E-009
2.129	0.0806	873.698	0.02377	1.8010E-009
3.037	0.1179	1278.028	0.02318	1.765E-009
3.945	0.1577	1709.457	0.02251	1.714E-009
–	–	–	0.02351	1.790E-009

The second method differed in the way that differences in piezometric heads Δh_{4-1} between measurement points 4 and 1 were computed. Since method 1 does not take into account measurements obtained for inner points 2 and 3, this time for each velocity inlet a linear function approximating piezometric heads was found. Differences Δh_{4-1} were computed based not on measured data, but on approximated values. Results are summarized in Table 4.

Table 4

Permeability coefficient calculations – method 2

$\vec{v_f} \cdot 10^{-3}$ [m/s]	Δh_{4-1} [m]	Δp_{4-1} [Pa/m]	K [m/s]	κ [m^2]
1.221	0.0440	429.651	0.024946	1.899E-009
2.129	0.0794	774.426	0.024135	1.838E-009
3.037	0.1165	1137.054	0.023449	1.785E-009
3.945	0.1561	1523.390	0.022736	1.731E-009
–	–	–	0.023816	1.813E-009

In methods 3 and 4 values of Δh_{4-1} are computed as in method 1 (Table 3). The pressure drops as a function of velocities are approximated with a linear function, its coefficient being equal to permeability. In method 3 no constraints

on a free-term were assigned, whereas method 4 assumed that the approximation line should pass through the origin of the coordinate system (free term equals zero). Results are given in Tabela 5.

Table 5

Permeability coefficient calculations – methods 3 and 4

Method	K [m/s]	κ [m^2]
Method 3:	0.02172	1.653E-09
Method 4:	0.02298	1.750E-09

If the permeability coefficient is known, the pressure drop between points 4 and 1 may be calculated according to (1). The impact of the method of data analysis is visualized in Figure 6. Errors due to methods 1 through 4 will be quantified in Part 2.

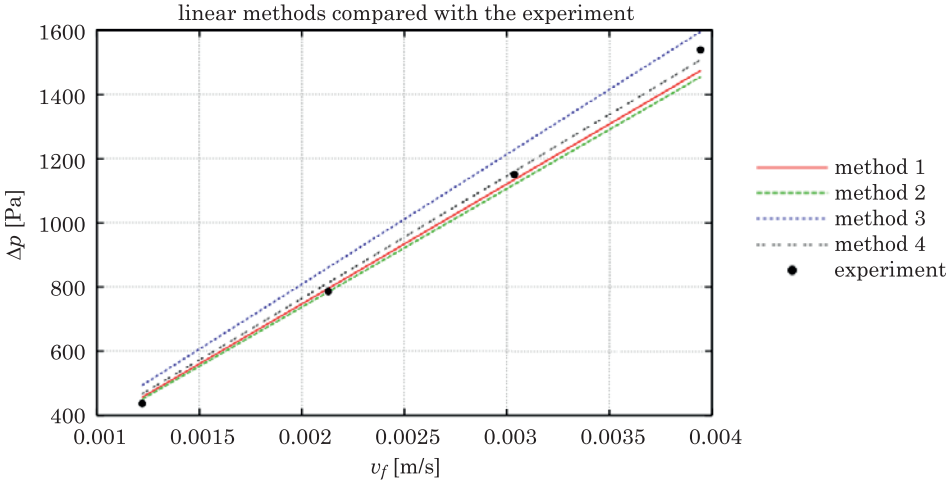

Fig. 6. Impact of data analysis on the agreement with the experiment for linear methods

Computation of porous media parameters – nonlinear model

In order to compute parameters κ and β based on experimental data, the Forchheimer Plot Method is used (HUANG, AYOUB 2008, ORODU et al. 2012, VAN BATENBURG, MILTON-TAYLER 2005). To this aim, the Forchheimer equation is rearranged to the form:

$$-\frac{\mathrm{d}p}{\mathrm{d}x}\cdot\frac{1}{\vec{v}_f\cdot\mu}=\frac{1}{\kappa}+\beta\left(\frac{\rho\cdot\vec{v}_f}{\mu}\right) \tag{9}$$

By introducing new variables:

$$\begin{cases} Y=-\dfrac{\mathrm{d}p}{\mathrm{d}x}\cdot\dfrac{1}{\vec{v}_f\cdot\mu} \\ X=\dfrac{\rho\cdot\vec{v}_f}{\mu} \end{cases} \tag{10}$$

a linear relationship is obtained:

$$Y=\beta\cdot X+\frac{1}{\kappa} \tag{11}$$

Measurement data were transformed following (10) and then parameters of a linear function (11) we are computed with the least-squares approximation. Two cases were distinguished. In Model A only data obtained for 6–12 measurement points (non-Darcy flows) were considered, whereas in model B also data obtained for slower flows (2–12) were taken into account (Fig. 7).

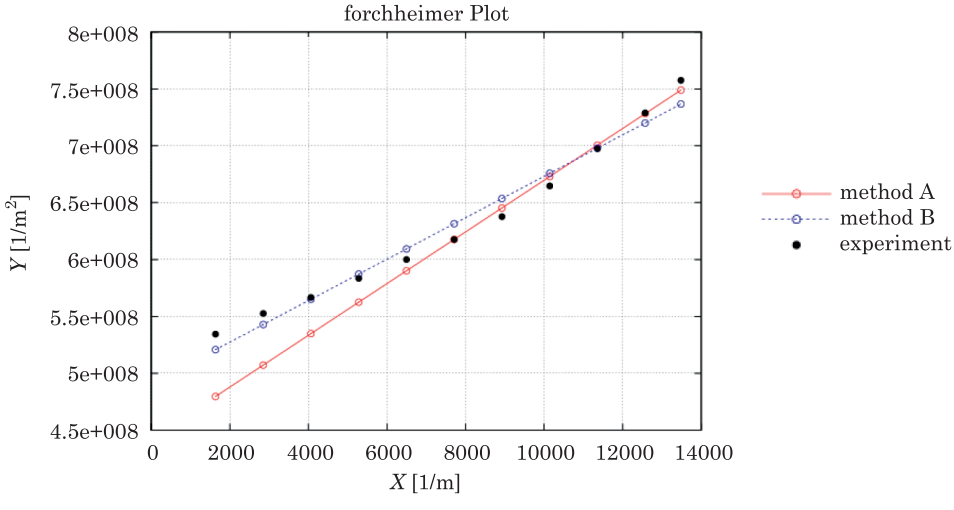

Fig. 7. Relationship between terms X and Y

An alternative way of computing parameters κ and β used original measurement data and was based on a least-square approximation with a quadratic function and a free term assumed to be zero. Again, two cases were

distinguished: Model C – based on non-Darcy flow data 6–12 only, and Model D, based on measurements 2–12. A summary of the computed parameters is given in Tabela 6. A comparison of non-linear methods and the experiment is shown in the Figure 8.

Table 6

Parameters κ and β computed with different methods

Method	K [m/s]	κ [m^2]	β [1/m]
Method A	0.02968	2.260E-09	22721.53
Method B	0.02675	2.037E-09	18215.36
Method C	0.03056	2.327E-09	23886.79
Method D	0.02874	2.188E-09	21569.43

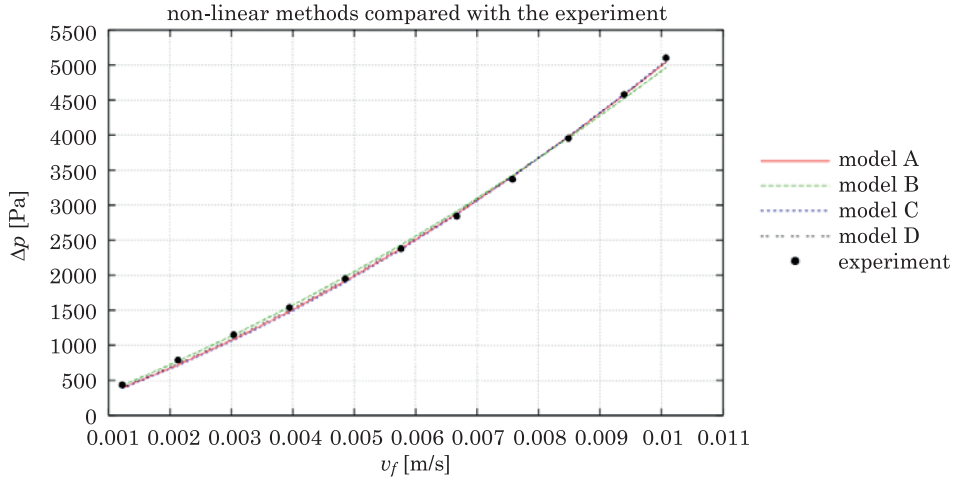

Fig. 8. Impact of data analysis on the agreement with the experiment for non-linear methods

Summary and conclusions

The range of flow rates covered by the experiment does not allow to precisely capture the onset of inertia effects. We have not got enough data belonging to the linear flow regime, what would be manifested by a constant ratio of flow rates and pressure drops. The rotameter characteristics did not let us to perform reliable experiments for lower flow rates. On the other hand, an attempt to make use of a graduated cylinder and a stop watch has proved not satisfactory, mostly due to instabilities in pressure drops observed during mesurements.

Thus the general conclusion is that in order to get a wider set of experimental data, an essentially different experimental set-up should be used. These will be a subject of our future works.

Due to practical difficulties mentioned above, we assumed here that the upper boundary of application of the Darcy law should be slightly above Re = 10. In this way we consider the flow cases from 2 to 5 (see Table. 1) to belong to the linear flow regime. This assumption does not introduce too much error, what is confirmed by the error analysis presented in the second part of the work.

As far as practical aspects of conducting measurements are concerned, the following remarks should be taken into account:

– The most important parameters are flow rates and pressure drops. Both should be measured with the highest available accuracy.

– In order to obtain higher quality of the data, every flow case (the same filtration velocity) should be repeated several times and then averaged (10 times seems to be enough, which is confirmed in Part 2 by small values of errors).

– The pressure drop should be measured over large sections of a sample. This would reduce the global error. The shorter measurement sections were, the higher was a difference between results and a line indicating the average (Fig. 3). However, in case of a nonhomogeneous layered packs, multiple mesurement points could be used to study local variations in pressure drops and to conclude about premeability variations.

– It is very important to keep the temperature constant during the experiment. This parameter does not appear explicitly in Darcy's, as well as Forchheimer law, but affects density and viscosity of the fluid. This conclusion was a result of our earlier investigations (SOBIESKI, TRYKOZKO 2011).

It is not possible to conclude which of the ways of data processing is the best for the mathematical model, which is shown in the Part 2. Our conclusions will be based on computations using numerical models and error analysis.

References

ALABI O.O. 2011. *Validity of Darcy's Law in Laminar Regime*. The Electronic Journal of Geotechnical Engineering, 16: 27–40.

ANDRADE J.S., COSTA U.M.S., ALMEIDA M.P., MAKSE H.A., STANLEY H.E. 1999. *Inertial Effects on Fluid Flow through Disordered Porous Media*. Physical Review Letters, 82(26): 5249–5252.

BATENBURG D. VAN, MILTON-TAYLER D. 2005. *Discussion on SPE 89325, Beyond beta factors: a complete model for Darcy, Forchheimer, and trans-Forchheimer flow in porous media*. JPT, 57(8): 72–73.

BEAR J. 1972. *Dynamics of Fluids in Porous Media*. Dover, New York.

CATALANO E. 2012. *A pore-scale coupled hydromechanical model for biphasos granular media*. PhD Thesis. University of Grenoble, France.

CHAPMAN R.E. 1981. *Geology and Water – An introduction to fluid mechanics for geologists*. Martinus Nijhoff & Dr. W. Junk Publishers, The Hague & Boston & London.

EWING R., LAZAROV R., LYONS S.L., PAPAVASSILIOU D.V., PASCIAK J., QIN G.X. 1999. *Numerical Well Model For Non-Darcy Flow*. Computational Geosciences, 3(3–4): 185–204.

HASSANIZADEH S.M., GRAY W.G. 1987. *High Velocity Flow in Porous Media*. Transport in Porous Media, 2(6): 521–531.

HELLSTRÖM J.G.I., LUNDSTRÖM T.S. 2006. *Flow through Porous Media at Moderate Reynolds Number*. 4th International Scientific Colloquium: Modelling for Material Processing. University of Latvia, Riga, Latvia, June 8–9.

HUANG H., AYOUB J. 2008. *Applicability of the Forchheimer Equation for Non-Darcy Flow in Porous Media*. SPE Journal, 13(1): 112–122.

ORODU O.D., MAKINDE F.A., ORODU K.B. 2012. *Experimental Study of Darcy and Non-Darcy Flow in Porous Media*. International Journal of Engineering and Technology, 2(12): 1934–1943.

PESZYŃSKA M., TRYKOZKO A. 2013. *Pore-to-core simulations of flow with large velocities using continuum models and imaging data*. Computational Geosciences, 17(4): 623–645.

SAWICKI J., SZPAKOWSKI W., WEINEROWSKA K., WOŁOSZYN E., ZIMA P. 2004. *Laboratory of Fluid Mechanics and Hydraulics*. Technical University of Gdańsk Publisher, Gdańsk, Poland (in Polish).

SOBIESKI W. 2010. *Use of Numerical Models in Validating Experimental Results*. Journal of Applied Computer Science, 18(1): 49–60.

SOBIESKI W., TRYKOZKO A. 2011. *Sensitivity aspects of Forchheimer's approximation*. Transport in Porous Media, 89(2): 155–164.

SUKOP M.C., HUANG H., ALVAREZ P.F., VARIANO E.A., CUNNINGHAM K.J. 2013. *Evaluation of permeability and non-Darcy flow in vuggy macroporous limestone aquifer samples with lattice Boltzmann methods*. Water Resources Research, 49(1): 1–15.

TINDALL J.A., KUNKEL J.R., ANDERSON D.E. 1998. *Unsaturated Zone Hydrology for Scientist and Engineers*. Pearson Education, New Jersey.

Technical Sciences 17(4), 2014, 337–350

DARCY'S AND FORCHHEIMER'S LAWS IN PRACTICE. PART 2. THE NUMERICAL MODEL

Wojciech Sobieski[1], *Anna Trykozko*[2]

[1] Department of Mechanics and Machine Design
University of Warmia and Mazury in Olsztyn
[2] Interdisciplinary Centre for Mathematical and Computational Modeling
University of Warsaw

Received 3 April 2014, accepted 8 November 2014, available on line 11 November 2014.

K e y w o r d s: Darcy's law, Forchheimer's law, Forchheimer Plot Method, porous media, permeability.

Abstract

Our study is based on a column experiment of water flow through a porous granular bed. In Part 1 we propose eight methods to derive parameters of flow models based on measurement data. These parameters are permeability and Forchheimer coefficient for Darcy's and Forchheimer's laws. The approach presented in this part uses two numerical models to perform simulations of flow. One model is based on the Finite Element Method implemented in the authors' code. The second model, which is ANSYS/Fluent package, uses the Finite Volume Method. Results of numerical computations are compared with experimental data that allows determination of the best method of parameter evaluation (in which the error was less than 3% over the whole range of filtration velocities). The problem of identification of ranges of applicability of the Darcy's and Forchheimer's laws is also addressed. In the conclusions, a set of guidelines is given, which should facilitate planning a similar experiment and its computational processing.

Introduction

In every experiment in which parameters are measured, and later used in a mathematical model, three main factors influence the quality of final results (SOBIESKI 2010b): precision of measuring equipment, a choice of a data processing method, and the accuracy of calculations. The current investigations are focused on the second aspect, in the context of modeling fluid flows through porous beds. Using different methods of data processing, we obtained several different values of permeability coefficient (Part 1). The aim of this

Correspondence: Wojciech Sobieski, Katedra Mechaniki i Podstaw Konstrukcji Maszyn, Uniwersytet Warmińsko-Mazurski, ul. M. Oczapowskiego 11, 10-957 Olsztyn, phone: +48 89 523 32 40, e-mail: wojciech.sobieski@uwm.edu.pl

paper is to apply numerical models in order to evaluate the quality of parameters. Numerical simulations reproducing the experiment were performed twice: based on the authors's code and applying the industry standard package ANSYS/Fluent (ANSYS Fluent 2014). Error analysis enabled the choice of the best method of data processing.

Numerical model of flow in porous media

The code we use solves the steady-state flow equation (BEAR 1972).

$$\nabla \cdot \left(\frac{\kappa}{\mu} \nabla p \right) = 0 \text{ in } \Omega \in R^3 \tag{1}$$

with
p – pressure [Pa],
κ – permeability [m^2],
μ – dynamic viscosity of the fluid [kg/(m · s)].

The permeability coefficient κ is a tensor in a general case (BREUGEM et al. 2004).

The domain Ω represents the column used in the experiments. Its boundary $\partial\Omega$ consists of three parts which are $\partial\Omega_{\text{wall}}$ – the side surface of the column, $\partial\Omega_{\text{out}}$ – the top of the column (outlet), and $\partial\Omega_{\text{in}}$ – the bottom of the column (inlet), $\partial\Omega = \partial\Omega_{\text{wall}} \cup \partial\Omega_{\text{out}} \cup \partial\Omega_{\text{in}}$.

The boundary conditions imposed on (1) are the following:

$$-\frac{\kappa}{\mu} \frac{\partial p}{\partial n} = 0 \text{ on } \partial\Omega_{\text{wall}} \text{ (no flow)} \tag{2a}$$

$$p = p_{\text{out}} \text{ on } \partial\Omega_{\text{out}} \tag{2b}$$

$$p = p_{\text{in}} \text{ on } \partial\Omega_{\text{in}} \tag{2c}$$

where p_{out} is a constant pressure on the outlet, p_{in} is a constant pressure on the inlet, both values are measured during the experiment.

Alternatively, one could replace (2c) with a condition imposing (a constant) flow rate v_{in} at the inlet, which is also available from the experiment:

$$-\frac{\kappa}{\mu}\frac{\partial p}{\partial n} = v_{\text{in}} \text{ on } \partial\Omega_{\text{in}} \tag{2d}$$

It is also possible to formulate equation (1) in terms of piezometric head h, $h = \frac{p}{\rho g} + z$, with denoting a fixed reference level, and conductivity coefficient **K** (Part 1, eq. 8). We assumed the reference level $z = 0$ is fixed at the bottom (inlet) of the pipe, thus the piezometric head at the outlet equals static pressure increased by the total length of the pipe. In particular, zero pressure at the outlet results in a piezometric head equal to the pipe's length.

Linear model

In order to solve (1) we applied Finite Element Method (FEM) (LUCQUIN, PIRONNEAU 1998) with linear basis functions constructed over tetrahedral elements. A cross-section of the computational domain is given in Figure 1. A mesh was created with the code Gambit (GAMBIT 2008), and then transformed to the format used by our code. As boundary conditions we used (2a), (2b), and (2d).

The system of linear equations was solved with a conjugate gradient method with a preconditioner based on incomplete Cholesky's decomposition (KAASSCHIETER 1988).

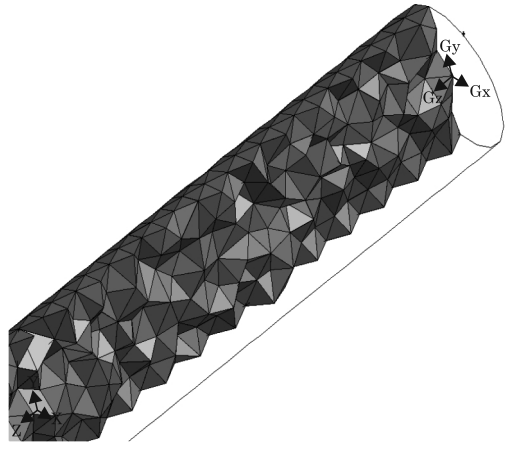

Fig. 1. Computational mesh – a cross-section

In a linear case filtration velocity $\vec{v}_f$ [m/s] can be obtained during a post-processing step using the Darcy's law:

$$\vec{v}_f = -\frac{\kappa}{\mu} \cdot \nabla p \tag{3}$$

Solution of Eqn. (1) with homogeneous coefficients defined over a cylindrical geometry and with boundary conditions (2) is a linear function. Even if the case under study could be described as a one-dimensional problem we have decided to consider a full geometry of the experimental column.

Nonlinear model

It is possible to extend the code to model flows described by the nonlinear Forchheimer law by adding an outer iterative loop (FOURAR et al. 2005).

The algorithm is based on Forchheimer's law (Part 1, Eq. 5) rewritten in the form

$$\vec{v}_f^{\,(i+1)} = -\kappa_{\text{eff}}^{(i)} \cdot \nabla p \tag{4}$$

where

$$\kappa_{\text{eff}}^{(i)} = \left(\frac{\mu}{\kappa} + \beta \cdot \rho \cdot |\vec{v}_f^{\,(i)}|\right)^{-1}, \quad i=1,... \tag{5}$$

with the upper index (i) denoting an iteration number. Since $\kappa_{\text{eff}}^{(i)}$ depends on $\vec{v}_f^{\,(i)}$ which is not known *à priori*, we start the procedure assuming $\kappa_{\text{eff}}^{(0)} = \frac{\kappa}{\mu}$ and solving Eq. 1, which gives the first approximation of the velocity field $\vec{v}_f^{\,(1)}$ (Eq. 4). Iterations follow the scheme: new approximations of permeability coefficient $\kappa_{\text{eff}}^{(i)}$ (5) are computed elementwise. Eq. (1) is solved with updated permeabilities, providing a new approximation of velocity field (4).

As boundary conditions on $\partial\Omega_{\text{out}}$ and $\partial\Omega_{\text{in}}$ we impose (2b) and (2c) which are pressures measured during experiment.

Iterations are repeated until convergence is reached. The stopping criterion is evaluated at each iteration step by comparing a newly computed velocity field and velocities obtained in a former iteration. This iterative scheme is not computationally optimal, but offers an easy way to get solutions of a nonlinear model.

It would be possible to reformulate the algorithm in such a way that the inlet boundary condition is defined by (2d).

As observed in (GARIBOTTI, PESZYŃSKA 2009), such an iterative approach fails to converge for highly heterogeneous media, in our case however we deal with a homogeneous medium. The more general approach to solve the Forchheimer equation is to apply the nonlinear Newton solver (GARIBOTTI, PESZYŃSKA 2009).

Simulation model based on ANSYS/Fluent package

ANSYS/Fluent is a widely-used commercial package to numerically solve fluid dynamics problems described by universal balance equations. The standard system of mass balance (6) and momentum balance (7) of a fluid (AALTOSALMI 2005, Fluent Inc. 2006, SOBIESKI 2010a), supplemented with an appropriate source term is used:

$$\frac{\partial}{\partial t}\rho + \nabla(\rho\vec{v}) = 0 \tag{6}$$

$$\frac{\partial}{\partial t}(\rho\ \vec{v}) + \nabla(\rho\vec{v}\otimes\vec{v}) = \nabla(-p\vec{\vec{I}} + \vec{\vec{\tau}}) + \rho\vec{s_b} \tag{7}$$

where:
ρ – density of the fluid [kg/m^3],
$\vec{v}$ – velocity [m/s],
$\vec{\vec{\tau}}$ – total stress tensor [Pa],
$\vec{s_b}$ – source of mass forces [N/m^3],
p – static pressure [Pa],
I – unit tensor [–].

As one of its features Fluent offers modeling flows in porous media by the Porous Media Model (PMM) (SOBIESKI 2011, SOBIESKI 2013). In the PMM approach an additional flow resistance, taking a form of a source of mass forces, is added to the source term of momentum balance equation (7). This source may be described by Darcy's law, what corresponds to losses due to viscosity

$$s_{i,viscous} = -\sum_{j=1}^{3} D_{ij} \cdot \mu \cdot v_j \tag{8}$$

or by Forchheimer's law, taking into account losses due to viscosity and inertia

$$s_{i,interial} = -\sum_{j=1}^{3} D_{ij} \cdot \mu \cdot v_j - \sum_{j=1}^{3} D_{ij} \cdot \frac{\rho \cdot |v| \cdot v_j}{2} \tag{9}$$

or any other law defining flow through porous media (ANDRADE 1999, ANSYS Fluent 2014, PATIÑO 2003).

Notation used in (8)–(9) follows the notation used in Fluent documentation (Fluent Inc. 2006). Symbol s_i denotes source of forces for the i-th space dimension (x, y, and in a 3D case), μ – dynamic viscosity coefficient [kg/(m.s)], v_j – the j-th component of velocity [m/s], $|v|$ – absolute value of velocity [m/s]. **D** is a matrix with diagonal terms equal to $1/\kappa$, and **C** is a matrix with diagonal terms equal to 2β. Off-diagonal terms in both matrices are null. It is possible to take into account anisotropic flows in ANSYS/Fluent by means of additional parameters, but it is not discussed here.

State variables of the system (6)–(7): pressure p and velocity $\vec{v}$ are independent, whereas the flow equation (1) depends on p only, and velocity $\vec{v}$ is derived from (3). In this sense, the system (6)–(7) represents a more general description of the process.

Table 1

Specification of computer model parameters

Parameter	Value or description
Solver	pressure based, steady
Computation domain type	3D
Energy equation	switched off
Viscous Model	laminar
Fluid	water
Fluid density	994.49 [kg/m^3]
Fluid viscosity	0.000743 [kg/(m · s)]
Operating pressure	101325 [Pa]
Gravitational acceleration	–9.81 [m/s^2]
Inlet type	velocity inlet
Inlet water velocity	0.0003127 – 0.0100738 [m/s]
Outlet type	pressure outlet
Outlet air pressure	0.0 [Pa]

The PMM described by equations (6)–(7) together with the source term should not be confused with a microscopic representation of a porous medium, where flow occurs in 'empty' void space (pores) of a medium and which is described by a set of Navier-Stokes' equations (as for instance in (PESZYŃSKA, TRYKOZKO 2013, VAKILHA, MANZARI 2008)). At a macroscopic scale these channels are not visible and averaged values are used instead. This is the case in the PMM applied in Fluent, which uses a source term in order to get averaged flow.

The geometry of the domain as well as the computational mesh were created with the Gambit package. Values of parameters used in Fluent are collected in Table 1.

Results and discussion

Simulations presented in this section were performed with the two codes described in sections 2 and 3. As parameters of the computational models we used experimentally-obtained parameters computed with all the methods proposed in Part 1, Sections 3 and 4.

Figure 1 gives the results of simulations obtained with the linear model and four different values of permeability computed with the four methods (Part 1, Sec. 3). We assumed that only four experiments (2–5) belong to the ranges of Darcy's law validity. A similar summary was performed for the nonlinear model with parameters described in Part 1, Sec. 4 (Fig. 2). In this case all filtration velocities $\vec{v}_f$ used in the experiment were taken into account. Numbers on plots denote measurement numbers and refer to Table 2 in Part 1. Results presented in Figs. 1 and 2 were obtained with the ANSYS/Fluent code.

Figures 1 and 2 allow comparison between static pressures obtained numerically and experimentally in measurement points along the column. In order to study the character of changes in pressure values between the extreme measurements points in function of filtration velocity, additional plots were made (Figs. 3 and 4), which will be referred to as flow characteristics. Figures 3 and 4 contain computational results obtained with the two codes. Since numerical results are identical, in further analysis and computations only results obtained with the ANSYS/Fluent code are considered. Software written by the authors was used to postprocess ANSYS/Fluent results, thus automating and significantly accelerating a single computation cycle.

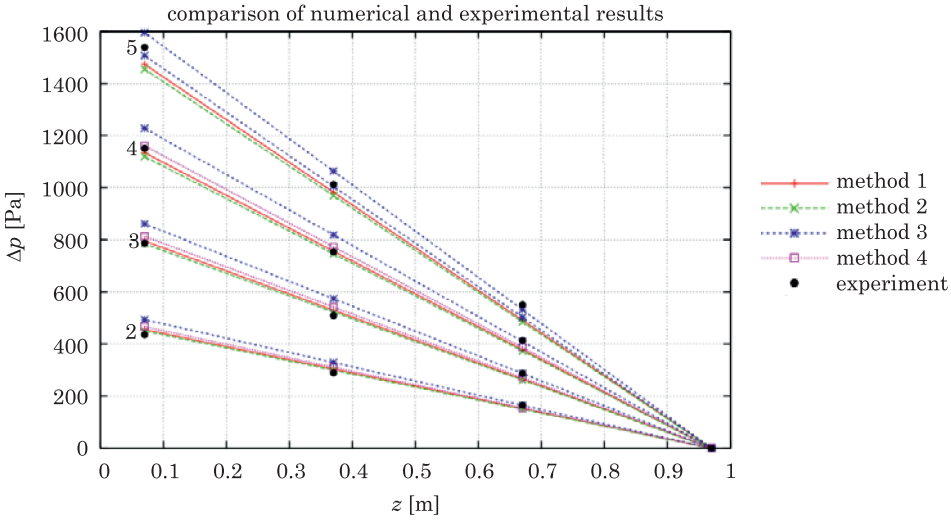

Fig. 1. Distribution of pressure along the column as a function of filtration velocity obtained by numerical simulations of linear model (continuous lines) and in measurements (points)

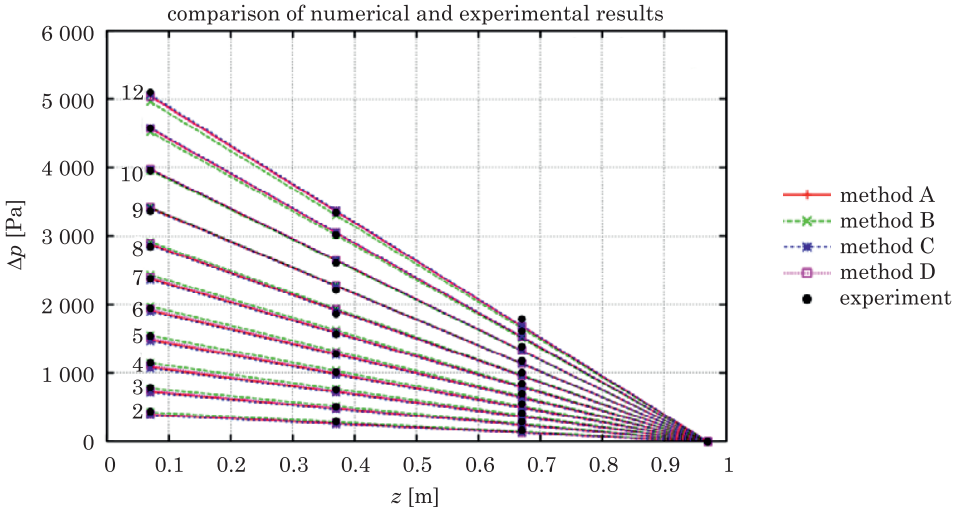

Fig. 2. Distribution of static pressure along the column axis as a function of filtration velocity obtained by numerical simulations of nonlinear model (continuous lines) and in measurements (points)

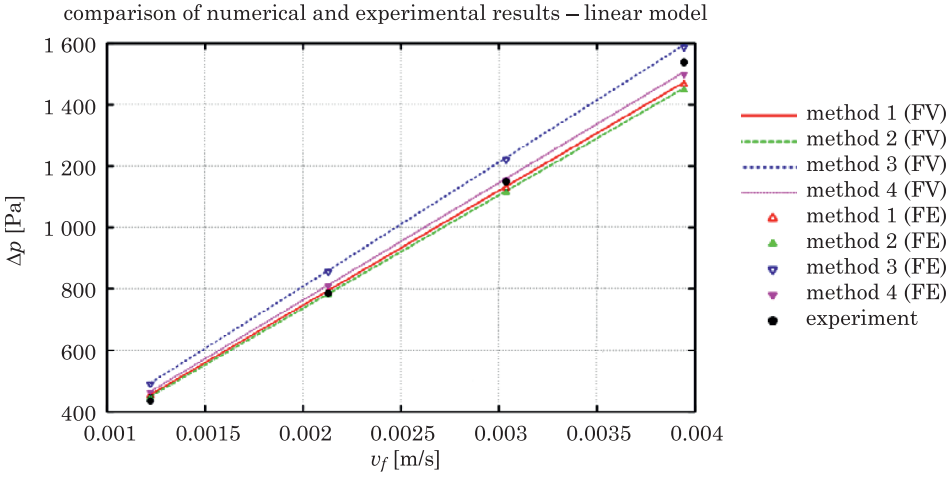

Fig. 3. Comparison of pressure drop as a function of velocity obtained numerically and experimentally for a linear model

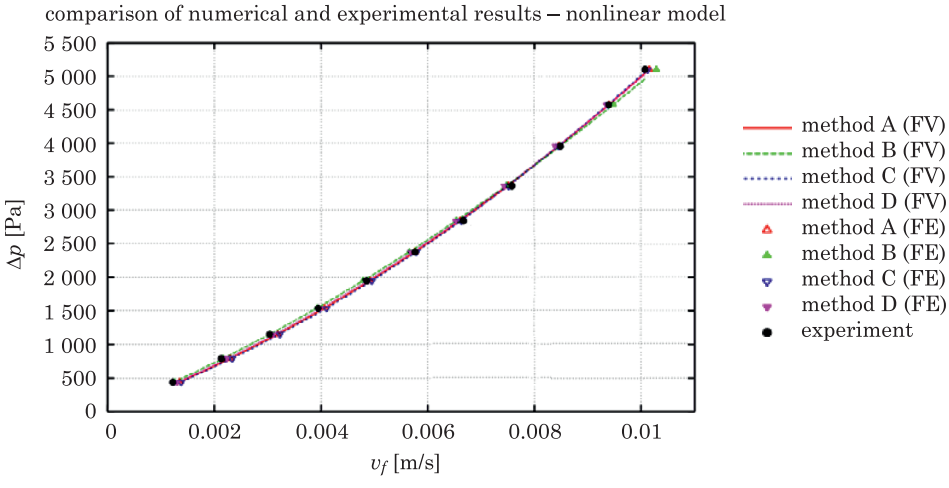

Fig. 4. Comparison of pressure drop as a function of velocity obtained numerically and experimentally for a nonlinear model

Error analysis

In order to find which of the methods used to compute model parameters provides the best agreement with measurements, an error analysis was performed. The percentage error δ_{i-0} was computed from the formula:

$$\delta_{i-0} = \left| \frac{x_i - x_0}{x_0} \right| \cdot 100\% \tag{10}$$

where:
x_i – numerically computed value of a state variable,
x_0 – the exact value (obtained experimentally).

Only directly measured values (as opposed to values obtained with approximation methods) were taken as x_0. Results for the four linear models (denoted with upper indexes) are given in Tables 2–4.

For the linear model, the error, reaching several percent, appeared for method 3 of permeability computation. Moreover, the flow characteristic is shifted upwards with respect to the measurement data, and all errors were of positive values. All remaining simulations, based on methods 1, 2, and 4, give similar results. Errors are smaller and of different signs. This error analysis shows that averaging methods perform better. Method 2 based on measurements at all measurements points along the column seems to be more relevant than method 1, or method 4, which is restricted to extreme measurement points.

Table 2

Percentage errors for a segment between measurement points 4 and 1

$\vec{v}_f$	$\Delta p^{\text{exp}}_{4-1}$	Δp^{1}_{4-1}	Δp^{2}_{4-1}	Δp^{3}_{4-1}	Δp^{4}_{4-1}	δ^{1}_{4-1}	δ^{2}_{4-1}	δ^{3}_{4-1}	δ^{4}_{4-1}
$\cdot 10^{-3}$ [m/s]	[Pa]	[Pa]	[Pa]	[Pa]	[Pa]	[%]	[%]	[%]	[%]
1.2207	436.09	455.90	450.04	493.54	466.36	4.54	3.20	13.17	6.94
2.1287	786.33	795.03	784.80	860.67	813.25	1.11	–0.19	9.45	3.42
3.0367	1150.22	1134.15	1119.56	1227.78	1160.15	–1.40	–2.66	6.74	0.86
3.9447	1538.51	1473.28	1454.32	1594.90	1507.05	–4.24	–5.47	3.66	–2.04

Table 3

Percentage errors for a segment between measurement points 3 and 1

$\vec{v}_f$	$\Delta p^{\text{exp}}_{3-1}$	Δp^{1}_{3-1}	Δp^{2}_{3-1}	Δp^{3}_{3-1}	Δp^{4}_{3-1}	δ^{1}_{3-1}	δ^{2}_{3-1}	δ^{3}_{3-1}	δ^{4}_{3-1}
$\cdot 10^{-3}$ [m/s]	[Pa]	[Pa]	[Pa]	[Pa]	[Pa]	[%]	[%]	[%]	[%]
1.2207	288.78	303.94	300.03	329.03	310.90	5.25	3.89	13.94	7.66
2.1287	509.26	530.02	523.20	573.78	542.17	4.08	2.74	12.67	6.46
3.0367	753.16	756.10	746.37	818.52	773.43	0.39	–0.90	8.68	2.69
3.9447	1012.67	982.18	969.55	1063.27	1004.70	–3.01	–4.26	4.10	–0.79

Table 4

Percentage errors for a segment between measurement points 2 and 1

$\vec{v}_f$	$\Delta p^{\exp}_{2-1}$	Δp^{1}_{2-1}	Δp^{2}_{2-1}	Δp^{3}_{2-1}	Δp^{4}_{2-1}	δ^{1}_{2-1}	δ^{2}_{2-1}	δ^{3}_{2-1}	δ^{4}_{2-1}
$\cdot 10^{-3}$ [m/s]	[Pa]	[Pa]	[Pa]	[Pa]	[Pa]	[%]	[%]	[%]	[%]
1.2207	164.88	151.97	150.01	164.51	155.45	–7.83	–9.02	–0.22	–5.72
2.1287	286.82	265.01	261.60	286.89	271.08	–7.60	–8.79	0.02	–5.49
3.0367	413.65	378.05	373.19	409.26	386.72	–8.61	–9.78	–1.06	–6.51
3.9447	550.23	491.09	484.77	531.63	502.35	–10.75	–11.90	–3.38	–8.70

As a next conclusion we get a confirmation of the assumption that the pressure drop should be computed based on the extreme measurement points. Using shorter segments between measurement points increases error values and results in a poorer quality of flow characteristics. This effect was already mentioned while discussing the influence of measurement point choice on the value of the permeability coefficient. A sequence of numerical simulations was performed (not described in this paper), with permeability coefficient computed based on pressure differences between measurement points 1–3, 2–4, and 2–3. The largest errors were encountered for the 2–3 case.

A visible difference of slopes of characteristics obtained for experiment and simulations is observed for the linear models (Fig. 3). This feature seems to be independent of the method of determining the permeability coefficient and may manifest the influence of other factors. It is possible that, in spite of relatively small Reynolds numbers, an influence of inertial losses is pronounced in our data (the same conclusion was stated in Part 1). This creates difficulty in defining the upper limit of Darcy's law validity with our results. Given our range of Re, this is consistent with the literature.

A similar error analysis performed for the nonlinear model indicates that method B provides the best values of coefficients for the Forchheimer equation. For the section between measurement points 4 and 1 (Table 5), errors for this method did not exceed 3%, which is a very good result. For the remaining methods, the errors were larger, in particular for smaller values of filtration velocity. Another indication in favor of method B is obtained by comparing averaged values of the absolute percentage error, which were for methods A, B, C, and D equal to 3.04, 1.57, 3.67 and 45%, respectively. As in the linear case, percentage errors were additionally computed taking into account shorter measurement segments. Again, a visible increase of errors followed a reduction the measurement segment length. Therefore measurements aimed at getting coefficients of nonlinear model should be conducted for the widest possible (available) range of filtration velocities, in spite of the range appropriate for the actual context of study.

Table 5

Percentage errors for computations based on nonlinear model

$\vec{v}_f$	$\Delta p_{4-1}^{\exp}$	Δp_{4-1}^{A}	Δp_{4-1}^{B}	Δp_{4-1}^{C}	Δp_{4-1}^{D}	δ_{4-1}^{A}	δ_{4-1}^{B}	δ_{4-1}^{C}	δ_{4-1}^{D}
$\cdot 10^{-3}$ [m/s]	[Pa]	[Pa]	[Pa]	[Pa]	[Pa]	[%]	[%]	[%]	[%]
1.2207	436.09	391.38	424.97	382.57	401.74	–10.25	–2.55	–12.27	–7.88
2.1287	786.33	721.81	772.60	708.46	737.89	–8.20	–1.75	–9.90	–6.16
3.0367	1150.22	1085.78	1147.10	1069.60	1105.87	–5.60	–0.27	–7.01	–3.86
3.9447	1538.51	1483.27	1548.50	1466.01	1505.68	–3.59	0.65	–4.71	–2.13
4.8527	1946.31	1914.32	1976.77	1897.66	1937.33	–1.64	1.56	–2.50	–0.46
5.7608	2378.50	2378.92	2431.98	2364.62	2400.87	0.02	2.25	–0.58	0.94
6.6688	2842.88	2877.04	2914.02	2866.79	2896.18	1.20	2.50	0.84	1.87
7.5768	3366.77	3408.67	3422.95	3404.21	3423.33	1.24	1.67	1.11	1.68
8.4848	3956.03	3973.85	3958.76	3976.89	3982.33	0.45	0.07	0.53	0.66
9.3928	4576.51	4572.55	4521.45	4584.81	4573.15	–0.09	–1.20	0.18	–0.07
10.0738	5101.38	5043.58	4961.11	5063.89	5037.15	–1.13	–2.75	–0.73	–1.26

Error analysis resulted in new data for a discussion on the limits of Darcy's and Forchheimer laws validity. Small errors encountered for the model B indicate that it is the most appropriate model to describe the flow within the whole velocity range.

Summary and conclusions

As a result of our studies a number of conclusions can be formulated:

– Forchheimer's law (with parameters computed with the Forchheimer Plot Method) gives better results for the whole range of flow velocities. For small Reynolds numbers, the contribution of the nonlinear term is small and the model becomes quasi-linear. Application of Forchheimer's law allows to avoid the error in estimating the flow regime – and the true character of flow is automatically manifested in simulations (provided a series of computations for a range of filtration velocities is performed).

– In spite of the latter statement, there exists a range of filtration velocities where linear models are an appropriate approximation and may be successfully applied. It is extremely important, because of a relative simplicity of linear models.

Our results suggest that for a wider range of different flow velocities relying only on Reynolds numbers and related literature-based upper bounds for Darcy's law validity may prove insufficient.

– To ensure a good quality of parameters, it is important to conduct as many measurements as possible for different filtration velocities. A single measurement (or a series but with the same parameters) may prove insufficient. Also, the larger range of filtration velocities is used in measurements, the more exact derived parameters are.

– Pressure drop should be defined based on measurements over the longest possible segment, fitted to a kind of a medium under study and a size of available samples. Taking shorter segments resulted in larger errors.

– Once parameters of a medium are known, simulating flow through a typical porous medium poses no problem. Several methods of computing permeability as well as Forchheimer coefficient were presented.

– It is essential to carefully measure piezometric heads (or pressures) in measurement points. Permeability coefficient is computed on their basis and the model is very sensitive to this parameter.

– Software used to model porous media may be based on a flow equation or on more general formulations of balance equations. A particular choice of a numerical method to solve equations (Finite Volume Method, Finite Element Method) seems not to have too much influence.

References

AALTOSALMI U. 2005. *Fluid Flow in Porous Media with the Lattice-Boltzmann Method*. PhD Thesis. Department of Physics, University of Jyväskylä. Finland, July.

ANDRADE J.S., COSTA U.M.S., ALMEIDA M.P., MAKSE H.A., STANLEY H.E. 1999. *Inertial Effects on Fluid Flow through Disordered Porous Media*. Physical Review Letters, 82(26), 5249–5252.

BEAR J. 1972. *Dynamics of Fluids in Porous Media*. Dover, New York.

BREUGEM W.P., BOERSMA B.J., UTTENBOGAARD R.E. 2004. *Direct numerical simulations of plane channel flow over a 3D Cartesian grid of cubes*. In: *Applications of porous media (ICAPM 2004).* Eds. A.H. Reis, A.F. Miguel. Evora Geophysics Center,. Évora, pp. 27–35.

ANSYS Fluent Home Page. 2014. On line:: http://www.ansys.com/Products/Simulation+Technology/Fluid+Dynamics/Fluid+Dynamics+Products/ANSYS+Fluent (access: 1 April 2014).

Fluent Inc. 2006. Fluent 6.3 User's Guide (September 2006), Chapter 7.19: Porous Media Conditions.

FOURAR M., LENORMAND R., KARIMI-FARD M. 2005. *Inertia Effects in High-Rate Flow Through Heterogeneous Porous Media*. Transport in Porous Media, 60(3): 353–370.

GAMBIT Home Page 2008. On line: http://www.fluent.com/software/gambit/index.htm (access: 1 March 2008).

GARIBOTTI C., PESZYŃSKA M. 2009. *Upscaling non-Darcy flow*. Transport in Porous Media, 80(3): 401–430.

KAASSCHIETER E.F. 1988. *Preconditioned conjugate gradients for solving singular systems*. Journal of Computational and Applied Mathematics, 24(1–2): 265–275.

LUCQUIN B., PIRONNEAU O. 1998. *Introduction to Scientific Computing*. Wiley. Chichester.

PATIÑO O.A.L. 2003. *Optimisation of Heat Sinks by Computational Flow Dynamics Techniques*. PhD Thesis. Gent University, Gent, Belgium.

PESZYŃSKA M., TRYKOZKO A. 2013 *Pore-to-core simulations of flow with large velocities using continuum models and imaging data*. Computational Geosciences, 17(4): 623–645.

SOBIESKI W. 2010a. *Examples of Using the Finite Volume Method for Modeling Fluid-Solid Systems*. Technical Sciences, 13: 256–265.

SOBIESKI W. 2010b. *Use of Numerical Models in Validating Experimental Results*. Journal of Applied Computer Science, 18(1): 49–60.

SOBIESKI W. 2011. *The Basic Equations of Fluid Mechanics in Form Characteristic of the Finite Volume Method*. Technical Sciences, 14(2): 299–313.

SOBIESKI W. 2013. *The Basic Closures of Fluid Mechanics in Form Characteristic for the Finite Volume Method*. Technical Sciences, 16(2): 93–107.

VAKILHA M., MANZARI M.T. 2008. *Modelling of Power-law Fluid Flow Through Porous Media Using Smoothed Particle Hydrodynamics*. Transport in Porous Media, 74(3): 331–346.

Technical Sciences 17(4), 2014, 351–360

ENERGY EFFECTS DURING USING THE GLASS WITH DIFFERENT PROPERTIES IN A HEATED GREENHOUSE

Sławomir Kurpaska

Institute of Agriculture Engineering and Informatics
University of Agriculture in Kraków

Received 8 July 2014, accepted 7 November 2014, available on line 11 November 2014.

K e y w o r d s: greenhouse, optic parameters of glass, heat consumption.

S u m m a r y

The paper presents results of calculations conducted on a change of demand for thermal power in a greenhouse covered with standard garden glass and a low-emission glass. Changes of heat demand were also determined. Changes of the amount of fuel (fine coal size grade) as well as changes in the emission of pollutants to the atmosphere were estimated based on calculations. It was determined that covering a greenhouse with low-emission glass has a positive impact on decreasing heat demand.

Introduction

A whole year cultivation of plants in greenhouses requires ensuring optimal parameters of microclimate (temperature, concentration of steam, concentration of the CO_2, light availability) on the one hand and reduction of production cost on the other. Both these aims may be reached not only using a suitable technical equipment of facilities but it may be assumed that a casing of a facility is also essential. A casing (glass, plastic) by proper isolation positively influences on the reduction of heat consumption as well creating proper conditions of light availability of wave length at which physiological processes occur in cultivated plants. Correct physical and optic properties of glass (thermal conductivity, reaction of glass surface on rays getting through) influence reduction of fuel consumption what brings measurable financial effects and reduction of pollutants emission to the atmosphere and increased profitability of production. Currently, there are well-prepared production

Correspondence: Sławomir Kurpaska, Instytut Inżynierii Rolniczej i Informatyki, Uniwersytet Rolniczy im. Hugona Kołłątaja, ul. Balicka 116B, 30-149 Kraków, phone: 48 12 6624628, e-mail: rtkurpas@cyf-kr.edu.pl

technologies and compiled methods of glass processing consisting in: modification of thermal properties as well optic parameters, which characterizes the flow of radiation of a suitable wave length (dusting metal coating or metal oxides on its surface), selective reflection of infrared radiation by application of low-emission glass, increasing a coefficient of light transmission by application of anti-reflexive glass. Estimation of potential benefits from using this type of processing or from using alternative (regarding glass) covering of a greenhouse is an essential challenge for science. This issue was the subject of the research. LEONIDOPOULOS (2000a, b) analysed energy issues in regard of a laboratory greenhouse covered with polymeric cover. As a result of the research, which he carried out and calculations he conducted, he determined daily kinetics of temperature change inside a facility for different levels of sun exposure. Moreover, he analysed the issue of thermo-dynamic balance as an effect of balancing of solar radiation energy with heat transmitted by a cover of the researched greenhouse in the process of its ventilation. AL-HELAL and ABDEL-GHANY (2011) determined quantitative heat fluxes used in a greenhouse (covered with PE foil) cooled with cooling mats divided into apparent heat and phase change. They divided solar radiation, which gets to a cover, into heat used in the processes occurring in a facility and into radiation reflected from the cover. TITEL et al. (2009) analysed heat consumption of a greenhouse (covered with PE foil) in which they installed a periodical heating system using warm air supplied to the inside with a system of perforated pipes. The authors found a relation between average temperature of leaves of the cultivated plants and temperature of their outer layer as well as a value of heat infiltration coefficient through a cover of a greenhouse for two cycles in its periodical heating. LI et al. (2009) compiled and verified a mechanistic model for prediction of air temperature in the system, in which warm water was stored between double foil covering the carcass of a greenhouse. It was concluded that the results obtained from the model give satisfactory comparison with intended values; co-participation of heat flux transmitted from the inside of a greenhouse to the outside was also determined. PISCIA et al. (2012) compiled a mathematical model (using CFD technology), which upon a verification procedure was used for simulation processes occurring on a casing of a greenhouse (a multi-nave tunnel covered with PE foil). The following issues were analysed: heat transfer by radiation from a tunnel casing to the surroundings, condensation of steam, plants transpiration and change of temperature of a casing during disappearance of solar radiation. It was concluded that a compiled model was useful for the analysis of fluctuations of air humidity inside a greenhouse. FIDAROS et al. (2010) worked out and verified a mathematical model for analysis of heat and mass transport phenomena in an air-conditioned greenhouse covered with PE foil. In a boundary condition (which

includes a surface of a cover and a surrounding), they considered heat transfer through convection and radiation. After the analysis was carried out, it was determined that the suggested model may be used for simulation of processes which occur in a greenhouse. ABDEL-GHANY and KOZAI (2006) using analogy between heat transfer and electric current transfer, prepared a mathematical model of processes, which takes place in a greenhouse covered with standard garden glass. The model includes the processes of heat transfer through radiation, conductivity and convection between a casing and the surroundings as well as between a casing and a surface layer of soil and air inside a greenhouse. Additionally, processes of air-cooling were included (through fog dispersal and gravitational ventilation). Values of particular heat fluxes mentioned among the analysed surfaces were determined and in conclusion after conduction of model verification, it was determined that the prepared model may be used in a further analysis of processes occurring in a greenhouse with cultivated plants and for finding coefficients of transfer. STANGHELLINI et al. (2011) analysed issues of radiation of near infrared (NIR) in a greenhouse in which screens of a high coefficient of reflection were installed. In conclusion, it was stated that installation of such screens reduces heat demand from greenhouses of about 8%. Application of dyes, the properties of which were determined in the research, was recommended for covering sidewalls in commercial greenhouses. In KURPASKA'S paper (2003) heat demand of a foil tunnel equipped in reflective screens (mounted behind heaters) as well as heat screens were analysed. HEMMING et al. (2011) analysed usefulness of garden glass (standard and low iron content) for improving its optic properties. As a result of analysis, which was carried out, it was determined that more considerable efforts will be obtained at modification of composite glass. The analysis, which was carried out, proved that positive effects (at current prices) will be also obtained for single glass in the case where its layer will be covered with an anti-reflexive cover. SONNENVELD et al. (2007) presented results of analysis using a modified cover of PE foil as a cover of photovoltaic boards. Boards were located in a roof of a laboratory greenhouse. Covering the foil with material characterised with selective permeability (in regard of NIR waves) of solar waves was the most crucial point of modification.

Relevance of the issue of modification of garden glass optic properties results from the performed review of the selected papers. The main purpose of this paper will be to carry out such an analysis (limited to thermal issues).

Material and methods

The subject of the analysis was to determine energy effects in a greenhouse covered with standard garden glass as well as glass of modified optic properties. Use of glass by changed optic parameters consists on covering a glass layer with an additional layer of strongly anti-reflection parameters (the so-called low-emission glass). Theoretically, this layer should influence reduction of heat consumption by a heated facility through reduction of infrared radiation. The analysis of heat losses from the inside of a greenhouse was conducted for the stationary state and temperatures of a heater T_g and a glass T_c averaged for the whole surface. In view of considerable sizes of these surfaces, a one-dimensional direction of heat flow from surfaces of heaters to the surroundings through a layer of air and glass may be accepted.

Figure 1 presents a schematic representation of a greenhouse with a mechanism of heat losses.

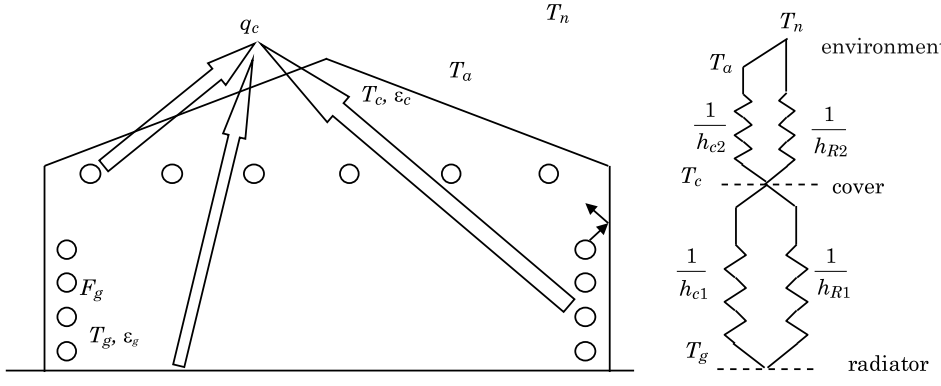

F_g – area of the heaters [m^{-2}],
T_g – temperature heating system [K],
ε_g – heaters emission factor [–],
T_c – temperature of greenhouse cover [K],
ε_c – greenhouse cover emission [–];
h_{c1}, h_{c2} – equivalent heat transfer coefficient by convection to the inner side (h_{c1}) and external (h_{c2}) of the greenhouse cover [$W \cdot m^{-2} \cdot K$],
h_{R1} – radiative heat transfer coefficient to the inner side (h_{R1}) and external (h_{R1}) of the greenhouse cover [$W \cdot m^{-2} \cdot K$],
T_a – ambient temperature [K],
T_n – sky temperature [K].

Fig. 1. Mechanisms of heat losses through a greenhouse casing along with an equivalent schematic representation of thermal resistance connections

A product of a relative difference of temperature and a substitutive coefficient of heat transmission may express convective losses from a heater to a glass, whereas relations for a hollow of surface area F_g and surrounding it F_c surface may express radiative heat exchange. In a methodology presented further (symbols occurring in relations are marked in Fig. 1), all parameters, material properties as well as listed heat fluxes are expressed in the international system of units.

For the above assumptions, the following relation expresses a total heat flux transmitted from a heater to a casing of a greenhouse:

$$q_{g-c} = q_{c1} + q_{R1} = h_{c1}(T_g - T_c) + \frac{\sigma(T_g^4 - T_c^4)}{\frac{1}{\varepsilon_g} + \frac{F_g}{F_c}\left(\frac{1}{\varepsilon_{c-ef}} - 1\right)} \tag{1}$$

where:
q_{c1} – heat flux transferred by convection, $W \cdot m^{-2}$,
q_{R1} – heat flux transferred by radiation, $W \cdot m^{-2}$;
σ – Stefan-Boltzman constant, $5.67 \cdot 10^{-8}\ W \cdot m^{-2} \cdot K^{-4}$,
ε_{c-ef} – stands for a weighted average of the emission coefficient (including glass surface area, cultivation surface area and their emissivity).

The same heat flux must be also diverted from a glass to the surroundings. Heat is conveyed through convection as well as emission to the sky. Thus, it may be expressed as follows:

$$q_{c-a} = q_{c2} + q_{R2} = h_{c2}(T_c - T_a) + \varepsilon_c\sigma(T_c^4 - T_n^4) \tag{2}$$

Introduce the substitutive coefficient of heat transmission through radiation between a heater and glass in the following form:

$$h_{R1} = \frac{\sigma(T_g^4 + T_c^4)(T_g + T_c)}{\frac{1}{\varepsilon_g} + \frac{F_g}{F_c}\left(\frac{1}{\varepsilon_{c-ef}} - 1\right)} \tag{3}$$

in addition, analogical for radiation between glass and the sky:

$$h_{R2} = \frac{\sigma\varepsilon_c(T_c^4 + T_n^4)}{T_c - T_a} \tag{4}$$

temperature of the sky (T_n) was calculated out of relation [LIN et al. 2009]:

$$T_n = 0{,}0522 \cdot T_a^{1,5} \tag{5}$$

according to a schematic representation of thermal resistance (Fig. 1), we will receive the substitutive coefficient of heat losses through the surface of glazing as:

$$U_c = \frac{1}{\frac{1}{h_{c1} + h_{R1}} + \frac{1}{h_{c2} + h_{R2}}} \tag{6}$$

thus, relation for describing density of heat losses stream between a heater and the surroundings takes the following form:

$$q_c = U_c(T_g - T_a) \tag{7}$$

From presented methodology, it clearly results that in order to determine heat losses from a facility, knowledge of temperature of a coating is required (T_c). It may be determined only by an iterative method, where a final stage results from an assumed accuracy of calculations.

Analysis of heat consumption was carried out for a heating season (September-May) based on frequency of the surroundings temperature occurrence in a differentiable time d_t, the amount of heat was determined from the following formula:

$$Q_c = U_c \cdot F_c(T_g - T_a)\, d\tau \tag{8}$$

Thus, total heat consumption in a heating season was calculated from the following relation:

$$Q_{\text{tot}} = \int_{\tau_1}^{\tau_2} LF \cdot U_c \cdot F_c(T_g - T_{a\text{–min}})\, d\tau \tag{9}$$

where:
F_c – surface of the greenhouse cover [m^2],
LF – the seasonal coefficient utilization of the maximum heating power [–],
τ_1 and τ_2 – stands for the analysed time interval in a heating season.

The ground of a greenhouse in both cases is covered with white foil PE of the emission coefficient equal to 0.8. Convective coefficients of heat transmission (h_{c1}, h_{c2}) were accepted according to an effective methodology (KURPASKA 2007).

Results and discussion

The analysis was carried out for a greenhouse of a usable area of 600 m^2, a casing index (surface area – usable area of a greenhouse ratio) equal to 2.0 and a cubic capacity of 3000 m^3. It was assumed that temperature in a greenhouse was 12°C, whereas its casing consists in a low-emission glass of a coefficient of long-wave radiation emission (NIR) on the level of $\varepsilon_{c1} = 0.18$, as well as alternatively standard glass of $\varepsilon_{c2} = 0.84$. Values of the final effective emission coefficient of a cover from the inside of a greenhouse were assumed as a weighted average (including a surface area of a cover and a usable area of a greenhouse) in calculations. Moreover, it was assumed that the surface area of heaters constitutes 35% of a usable area of a greenhouse, while an emission coefficient of heaters is $\varepsilon_g = 0.94$. Heat flux exchanged between the inside of a greenhouse and surroundings through infiltration was calculated in calculations regarding heat consumption using standard relations. Figure 2 presents impact of surroundings temperature on the value of the coefficient of heat transfer.

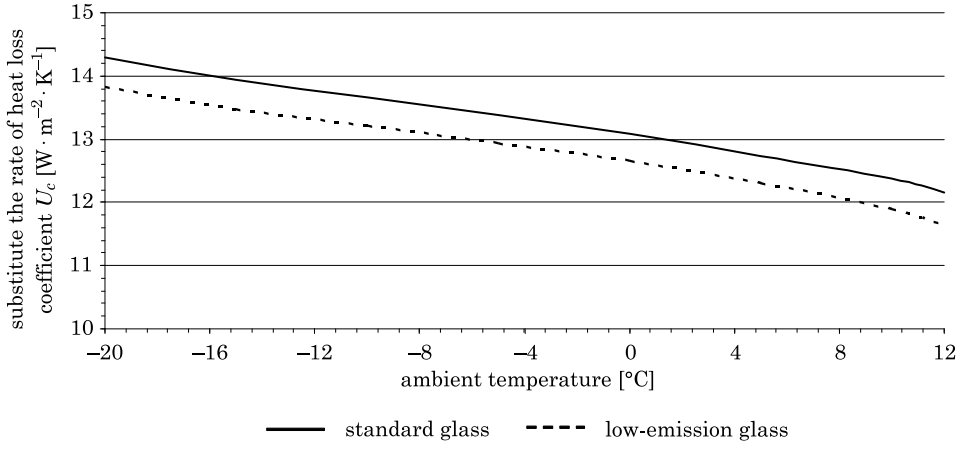

Fig. 2. Change of heat losses coefficient for the analysed casings

As it can be seen, glass of lower emission is characterised by a lower emission coefficient and by a lower value of the substitutive heat losses

coefficient. For the analysed scopes of independent variables, this coefficient for the low-emission glass in comparison to glass of standard emission takes on average 3.5% of lower value.

Figure 3 presents the influence of independent variables (the coefficient of glass emission, temperature of heaters) on the change of a unitary heat demand for the researched greenhouse. A linear change of heaters temperature depends on the temperature of surroundings.

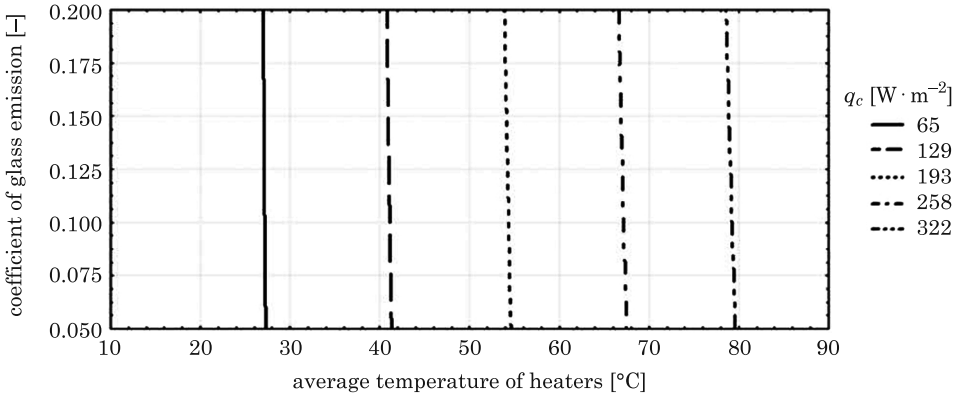

Fig. 3. Influence of heaters temperature and the coefficient of glass emission on unitary heat demand

It may be noted that the higher value of coefficient of emission is the higher unit demand for a heat flux. In the research scope of changes of the value of the heat emission coefficient (scope of changes within 0.05 to 0.2), a calculated variable (in regard to demand for a minimal value of emission) constitutes 1.9%.

A demand for thermal energy in the analysed greenhouse facility was calculated based on the relation, which presents frequency of the outside temperature for the sphere III (SZARGUT, ZIĘBIK 1995). Results of calculations were presented in Figure 4.

Because of similar courses of changes thermal loads for both analysed casings, (change a thermal load is a derivative of changes the value of heat losses coefficient) the course of loads was presented for a greenhouse covered with glass of standard value heat emission. A calculated value of *LF* coefficient is 0.26.

Thus, calculation results in the amount of heat necessary in the heating season for a greenhouse covered with the analysed casings were presented in Table 1.

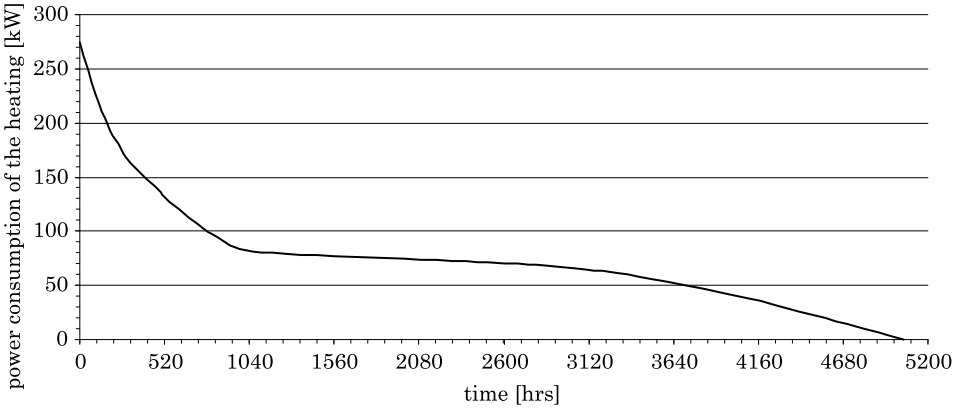

Fig. 4. An arranged diagram of thermal loads for the researched facility

Table 1

Amount of heat in the heating season

Type of casing	Heat demand [GJ · greenhouse^{-1} · a^{-1}]
Standard glass	1218.05
Low-emission glass	1171.85

Assuming that a greenhouse will be heated with fine coal size grade and assuming that total heat losses constitute 20% (transfer losses, losses in a boiler room) over 2.5 tons of fuel will be saved in the analysed greenhouse. Certainly, emission of pollutants to the atmosphere will be also reduced of CO_2 – 4264; CO – 47; SO_2 – 18; NO_x – 3.9 as well as dust of approx. 25 kg.

Conclusions

1. In the researched scope of independent variables, glass of lower emission in comparison to standard glass is characterised with the coefficient of heat losses, which is lower of 3.5%.

2. In the analysed facility, a unitary demand on heat decreases of approx. 2% along with the increase of the coefficient of glass emission (within the range of 0.05 to 0.2).

3. In the researched greenhouse, the use of low-emission glass leads to over 2.5 tons of fuel as well as reduction of pollutants emission to the atmosphere.

References

Abdel-Ghany A.M., Kozai T. 2006. *On the determination of the overall heat transmission coefficient and soil heat flux for a fog cooled, naturally ventilated greenhouse: Analysis of radiation and convection heat transfer*. Energy Conversion and Management, 47: 2612–2628.

Al-Helal I.M., Abdel-Ghany A.M. 2011. *Energy partition and conversion of solar and thermal radiation into sensible and latent heat in a greenhouse under arid conditions*. Energy and Buildings, 43: 1740–1747.

Fidaros D.K., Baxevanou C.A., Bartzanas T., Kittas C. 2010. *Numerical simulation of thermal behavior of a ventilated arc greenhouse during a solar day*. Renewable Energy, 35: 1380–1386.

Hemming S., Kempkes F.L.K., Mohammadkhani V. 2011. *New glass coatings for high insulating greenhouses without light losses – energy saving crop production and economic potentials.* Acta Horticulturae, 893: 217–226.

Kurpaska S. 2003. *Modification of the technical equipment of the tunnel in terms of its foil heat demand*. Problemy Inżynierii Rolniczej, 1: 39–46.

Kurpaska S. 2007. *Greenhouses and plastic tunnels-engineering processes*. PWRiL, Warszawa.

Leonidopoulos G. 2000a. *Greenhouse daily sun-radiation intensity variation, daily temperature variation and heat profits through the polymeric cover*. Polymer Testing, 19: 813–820.

Leonidopoulos G. 2000b. *Greenhouse dimensions estimation and short time forecast of greenhouse temperature based on net heat losses through the polymeric cover*. Polymer Testing, 19: 801–812.

Li S., Willits D.H., Browdy C.L., Timmons M.B., Losordo T.M. 2009. *Thermal modeling of greenhouse aquaculture raceway systems*. Aquacultural Engineering, 41: 1–13.

Piscia D., Montero J.I., Baeza E., Bailey B.J. 2012. *A CFD greenhouse night-time condensation model*. Acta Horticulturae, 111: 141–154.

Sonneveld P.J., Holterman H.J., Swinkels A.M., van Tuijl B.A.J., Bot G.P.A. 2007. *Greenhouse with an integrated conentrated PV system*. Procc. 22nd Photovoltanic Solar Energy Conference, Milano.

Stanghellini C., Dai J., Kempkes F. 2011. *Effect of near-infrared-radiation reflective screen materials on ventilation requirement, crop transpiration and water use efficiency of a greenhouse rose crop*. Acta Horticulturae, 110: 261–271.

Szargut J, Ziębik A. 1995. *Fundamentals of thermal energy (in Polish)*. WNT, Warszawa.

Teitel M., Barak M., Antler A. 2009. *Effect of cyclic heating and a thermal screen on the nocturnal heat loss and microclimate of a greenhouse*, Biosystems Engineering, 102: 162–170.

Technical Sciences 17(4), 2014, 361–370

ANALYSE OF THE DURABILITY OF ASH-CEMENT COMPOSITES WITH FLY ASHES FROM THE HEAP MICHELIN POLAND SA SUBJECTED TO CORROSION

Andrzej Rudziński

The Chair of Engineering Materials and Building Processes
University of Warmia and Mazury in Olsztyn

Received 21 August 2014, accepted 20 November 2014, available on line 24 November 2014.

K e y w o r d s: fly ashes from the heap, hydrates lime, corrosion.

A b s t r a c t

Useless waste materials are often stored in urban areas taking valuable land and polluting the environment. There has been undertaken research which aim was to test the applicability of the ashes from multi-year heaps as a partial substitute for sand. In the ash-cement composites 10%, 20% and 30% weight of sand was replaced by an ash. Composites sand-ash-cement was modified by an addition of hydrated lime. Introduction of new materials environmentally friendly, using industrial waste is desirable when by using waste materials there is a possibility to obtain materials with desired, assumed technical characteristics and durability. The 30-day trials were subjected to corrosion in 6% solution of sodium chloride and magnesium sulfate. After the corrosion designated the compressive strength of each series, which compared with strengths of series in the same age and not subjected to corrosion. Generally, all composites with the ashes scored higher compressive strength in the control series – without ash. The presence of ash in composites significantly reduced the effects of corrosion. These results suggest the possibility of using these composites in road construction.

Introduction

Power engineering in Poland is mainly based on coal combustion. In 2012 Poland prepared 135,209,000 tons of waste materials including combustion by-products (ash and slag) accounted for approximately 10%. In the Warmia-Mazury made at this time 815 300 tonnes of waste materials, including fly ash accounted for 5.10% of all waste materials (*Environment protection* 2013).

At the turn of the twentieth and twenty-first centuries a result of efforts to sustainable development great importance is attached to the disposal of industrial waste. The result of these trends, a large percentage of by-products

Correspondence: Andrzej Rudziński, Katedra Materiałów i Procesów Budowlanych, Uniwersytet Warmińsko-Mazurski, ul. Heweliusza 4, 10-724 Olsztyn, phone: 48 89 523 47 18,
e-mail: andrzej.rudzinski@uwm.edu.pl

of combustion is regularly used in various sectors of the economy especially in the building engineering. By-products of combustion (BC) are a valuable component of cement. This applies, unfortunately, only the ashes collected from the electrostatic precipitators. For decades, the ashes – by-products of coal combustion were collected in heaps, often in areas or near cities and were troublesome waste. Development of ash rising. However, people should look for new uses of ash, which involves the study of this group of waste (KRUGER 2005, SVOBODA et al. 2007). Fly ashes that remain for many years in landfills still represent a big problem for local residents and local governments. This problem did not pass Olsztyn – the city of a typical tourist.

Rational utilization of the combustion by-products, the development and dissemination of new technologies to produce goods will always be up to date.

There is thus justified by the need for greater use of ashes, among other things, as an addition to the fine-grained composites made with sand, cement and ashes. Increasingly becoming too noticeable deficit irreproducible coarse-grained mineral aggregates, which leads to greater use of sands, which are still widely available raw material.

In the present study performed a series of tests with a limited amount of mortar cement, in which the ash from a heap replaced a part of sand. Mortars modified with hydrated lime in an amount of 4 to 6% by weight of ash added.

The aim of this study was to optimize the composition and determine the durability of composite sand-ash-cement with fly ash from long-term heap local origin subjected to corrosion. In this work were used as the corrosives solution of 6% of sodium chloride and magnesium sulfate. The introduction of new technologies environmentally friendly with the use of industrial waste is expedient if there is possible to get the materials with expected technical properties and durability.

Materials and methods

The following materials were used for tests:

– natural sand with a particle size 0–2 containing 81.5% quartz, chalcedony and opals, 12% of the igneous and metamorphic rocks, 5.3% sedimentary rocks with the alkaline reactivity of 0;

– fly ash heap of long-term loss on ignition approximately 15%, with about 60% of a fraction 0,063–0,5 mm with CaO containing about 2%;

– Portland cement CEM I – 32.5R;

– hydrated lime;

– 6% solutions of NaCl and $MgSO_4$;

– distilled water.

With these ingredients made a series of sand and ash and cement mixtures. As the series 0 adopted the qualitative composition similar to mortar Standardization (by determining the class of cement), but the plot frame sand was replaced with natural sand and were reduced by 80% weight of the cement (from 450 g to 90 g). Natural sand by the composite with addition of ash equal to 10%, 20%, and 30% by weight of sand was replaced.. The composites with the addition of fly ash modified with the addition of hydrated lime at 4 and 6% by weight of added ash (series 1.4, 1.6, 2.4, 2.6, 3.4 and 3.6). Calcium hydroxide was distributed in the make-up water. Volume of water in each series of tests were experimentally selected to obtain a constant consistency of composites.

Qualitative and quantitative composition of respondents series of tests are presented in Table 1. In all series of tests was performed to study the compressive strength after 30 and 90 days of setting and hardening (Tab. 2). There are also shown changes in the compressive strength of 90 days in relation to the strength 30 days old samples (Fig. 1).

Table 1

Qualitative and quantitative composition of composites

Series	Sand	Ash	Water	Hydrated lime	
				4% by weight of ash	6% by weight of ash
	g		cm^3	g	
0	1350	–	142	–	–
1.4	1215	135	167	5,4	–
1.6	1215	135	167	–	8,1
2.4	1080	270	167	10,8	–
2.6	1080	270	167	–	16,2
3.4	945	405	191	16,2	–
3.6	945	405	191	–	24,3

The weight of cement in all series of tests has become 90 g
Source: own research

Corrosion resistance test was conducted of all series of tests of composites. As corrosive media were used:

– 6% sodium chloride solution;
– 6% magnesium sulfate solution.

Capacity of the above solutions, in which the samples were immersed equal to 1.5 volumes of tested samples. During the test solutions were not exchanged, and in the case of evaporation it was supplemented with distilled water to a constant volume. Changes in the concentration of the solutions had to be only the result of reaction with components of the composite. Operation of corrosive

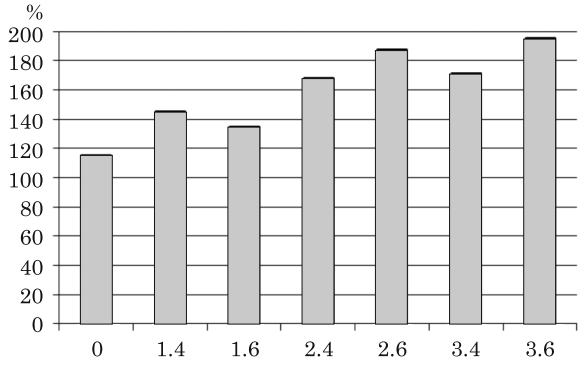

Fig. 1. Change of the compressive strength 90-day old samples in relation to the strength of the trial 30-day old samples

Source: own research.

solutions was carried out in a static system. Effects of 60-day interaction of NaCl and $MgSO_4$ solutions for cement-fly ash composite was determined by measuring the compressive strength f_{cm}.

The obtained values of the compressive strength after corrosion of the samples were compared to corresponding values of the tested samples at the same age not subjected to corrosion.

Discussion of the results

The results (Tab. 2) confirm the fact that the processes of hydration of fly ash-cement mixtures are slower than made of pure cement (BENTZ, FERRARIS 2010). With a very limited amount of cement in the hydration reaction is formed a small amount of calcium hydroxide. The ash content in all series of tests significantly exceeded cement content. There was added calcium hydroxide in an amount of 4 to 6% by weight of cement to enable the reaction of pozzolanic of ash, with about 2% of CaO, which may be insufficient to each series of tests, (GARCIA-LODEIRO et al. 2013). Significant increases in the compressive strength of composites of ash and sand-cement samples were obtained for the 90 day tests compared to 30 days. Changes in the compressive strength series 1.490/1.430 are almost 45% while the strength of the reference mortar without ash after the same period of time has increased by less than 15%.

The highest changes in the strength of 90-day trials in relation to the 30-day trials were obtained for a series 2.6 and 3.6 of 187 and 195% (Fig. 1).

In recent years, great attention is paid to testing the durability of materials, especially those made of cement (KURDOWSKI 2010, NEVILLE 2012). The reason

for interest in sustainability is big air and water pollution. Associated with that the aggressiveness of the environment increases the rate of corrosion reaction. The presence of fly ash in building material should not result in corrosive solutions for greater destruction than is the case in the material made of conventional materials. Applied in research NaCl and $MgSO_4$ solutions are typical corrosive media, which are exposed construction materials.

Chloride salts are harmful to the cement matrix. Chloride aggression is mainly connected with the action on materials commonly used de-icing agents. The most commonly temperature lowering compound is a low-grade (2% and 3%) solution of sodium chloride. To obtain the effect of corrosion at higher concentrations in a shorter time applied in the study 6% sodium chloride solution in which were immersed tested series for a period of 60 days. The corrosion of the composite cement and fly ash requires the transport of reactive ions to the reaction space, it means to the inside of the composites.

This may take place generated by two mechanisms:

– migration, flow to the inside of the composite as a result of capillary (SPIESZ, BROUWERS 2013);

– diffusion of ions as a result of a concentration gradient in different areas (AMARNATH et al. 2011).

The first mechanism has a much higher speed of transport, which entails a rapid progress of corrosion. The role of large capillary pores in the acceleration of corrosion is evident. The diffusion coefficient D decreases and salt concentration increasing in time, which is caused by the progressive hydration of the cement (HA-WON et al. 2008). Assessing the migration process in the hardened cement paste, and probably also in the ash-cement composites should be aware that this is not a pure diffusion. Diffusing ions react with the grout phases and are adsorbed on the amorphous surface of the phase C-S-H. Chloride ions also react with hydrated calcium aluminates giving Friedel's salt ($C_3A \cdot CaCl_2 \cdot 10H_2O$). This compound does not cause expansion, on the contrary reduces the amount of generated expansive compounds (CHALEE et al. 2007, KURDOWSKI 2010, AMARNATH et al. 2011).

Chloride corrosion in the present study examined composites sand and ash-cement decreased their compressive strength. The highest decreases in strength was observed in the control sample (without ash) – 27%. The increase of ash and calcium hydroxide in the composites affected favorably on the corrosion resistance. In the series of tests with the6% addition of lime, and increasing amounts of ash 10, 20, 30% after the corrosion reported lowest declines of endurance equal 11.5%, 11.1% and 7.0% (Fig. 2). Increasing amount of ash with the addition of lime proofed composites to chloride corrosion.

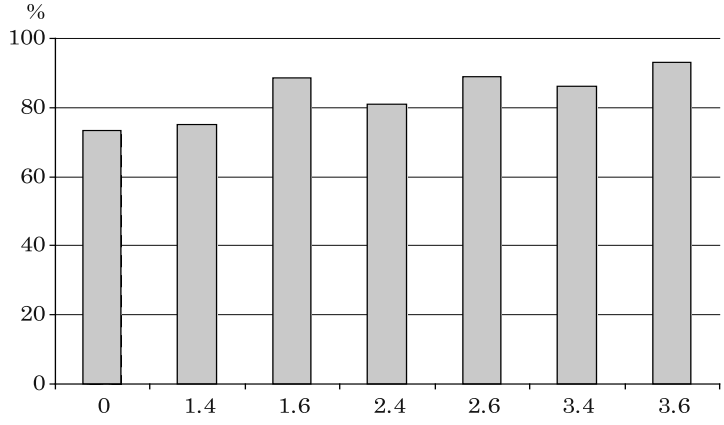

Fig. 2. Change of compressive strength of samples after 60 days of corrosion at 6% NaCl solution in relation to the samples of the same age not subject to corrosion
Source: own research.

$MgSO_4$ corrosive action causes not only sulfate corrosion, but also magnesium. Hydration products of ash-cement composites contain significantly less calcium hydroxide. During penetration of composites with ash by solutions containing sulfate ions an important role played pore size, the content of aluminum oxide and calcium oxide included in ashes. They may participate in the reaction with sulphates, especially when Al_2O_3 and CaO are present in the enamel of fly ash, thus providing a source of material which reacts with sulphates. The high ratio of silica to aluminium oxide reduces the sensitivity of the binder with ash on sulfate aggression but it is not completely proven (NEVILLE 2012).The reaction products of magnesium sulfate with calcium hydroxide, which is formed by binding the alite and belite, are sequentially calcium sulfate, calcium sulfate, dehydrate calcium sulfate, which in the presence of C_3A passes to ettringite. In addition there also arises brucite. Brucite can settle in the pores thereby forming at the surface of composite protective layer, which prevents further penetration of sulphate and magnesium ions to the interior. Generally concretes made with cement containing the ashes are characterized by increased resistance to aggressive agents. These properties intensify with increasing ash content in the composite. In the case of sulfate corrosion intensity decreases with decrease of C_3A (KURDOWSKI 2010). Large water and air pollution by sulfur oxides, from which arises sulfuric acid and its salts, causes the sulphate corrosion of building materials from many years has been a subject of many scientific studies (MARCHAND et al. 2002, SANTHANAM et al. 2006, SAHMARAN et al. 2007, BASSIST, WĘGLEWSKI 2009, TKACZEWSKA, MAŁOLEPSZY 2009, LOTHENBACH et al. 2010, LORENTE et al. 2011, SCHMIDT et al. 2012, RUDZIŃSKI 2013). The authors of mentioned works as

Table 2

Compressive strength of composite sand-ash-cement before and after corrosion

Series	Compressive strength				Absorbability [%]
	before corrosion		after corrosion		
	30-day trials	90-day trials	6% NaCl	6% $MgSO_4$	
0	1.3	1.5	1.1	1.2	12.6
1.4	2.2	3.2	2.4	2.5	13.3
1.6	2.6	3.5	3.1	3.0	13.2
2.4	2.5	4.2	3.4	3.8	16.5
2.6	2.4	4.5	4.0	4.1	16.8
3.4	2.1	3.6	3.1	3.7	21.1
3.6	2.2	4.3	4.0	4.3	21.4

Source: own research.

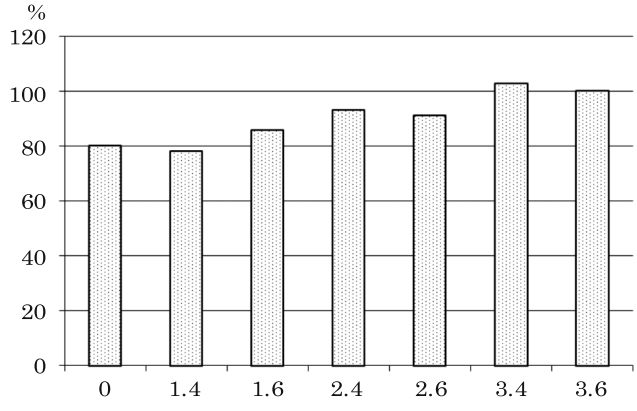

Fig. 3. The change of compressive strength of samples after 60 days corrosion in the 6% solution of $MgSO_4$ relative to the samples of the same age not subjected to corrosion

Source: own research.

corrosive solutions have used sulfate salt shaving different concentrations, wherein the concretes and mortars were subjected to corrosion for different periods of time (from several days to several years).In the present work sand-ash-cement composites were subjected by 60 days of action 6% magnesium sulfate solution. As in the case of chloride corrosion the lowest compressive strength was obtained after corrosion for a control series without ash and for a series with the lowest addition of ash and lime (Tab. 2, Fig. 3). Strength of test control series after sulfate-magnesium corrosion fell by 20%. Strength of the composites with 20% exchange sand by ashes fell by only a few percent. Strength of the 30% share of the ashes instead of sand after the corrosion practically did not change resistance, both from 4 and 6% with addition of lime (Tab. 2, Fig. 3).The composites with 30% conversion of the

sand by ash from both the 4 and 6% with addition of lime – a series of 3.4 and 3.6, practically after the sulfate-magnesium corrosion did not change their strength.

Conclusions

The obtained results allow to conclude that:

– generally much higher compressive strength values obtained for a series of 90-dayssamples of sand-ash-cement composites as compared to strengths of 30-day samples;

– ash-sand-cement composites in which the ash from the heap was used as a partial replacement for sand have much higher strength than the ash-free composites with the same amount of cement;

– the effects of corrosion processes samples treated with 6% NaCl solution are significantly lower in composites with fly ash than in the control series of „0" – with no ash;

– corrosive action of 6% $MgSO_4$ solution that exposes concrete and mortar to magnesium and sulphate corrosion is weaker than in during of chloride corrosion – in the composite in which 30% of the sand was replaced with ash from the heap did not noted any negative effects of sulfate-magnesium corrosion.

Conclusions

Generally much higher compressive strength values obtained for a series of 90-days samples of sand-ash-cement composites as compared to strengths of 30-days samples, which amounts to a series of attempts – 1.4 – 45%, for 2.6 and 3.6 – 187% and 195%, and for the series without ash – only 15%.

Ash-sand-cement composites in which the ash from the heap was used as a partial replacement for sand have much higher strength than the ash-free composites with the same amount of cement. In a series of 90-days samples strength of the series 0 is only 1.5 MPa and in series with ashes from 3.2 to 4.5 MPa.

The effects of corrosion processes samples treated with 6% NaCl solution are significantly lower in composites with fly ash than in the control series of „0" – with no ash. Minimal reduction in the compressive strength after corrosion – 11.1% and 6.8% were obtained for a series of tests with 20 and 30% conversion of the sand to ash, while the strength of the control series dropped by 27%.

Corrosive action of 6% $MgSO_4$ solution that exposes concrete and mortar to magnesium and sulphate corrosion is weaker than in during of chloride corrosion. In the composite in which 30% of the sand was replaced with ash from the heap did not noted any negative effects of sulfate-magnesium corrosion. In the series of the control sample and 10% content of the ash compressive strength decreased by about 20%.

Conversion of 20% and 30% sand to ash in the ash-cement-sand composites with a very limited amount of the cement significantly reduces the effects of corrosion in the test.

References

AMARNATH Y., GANESH B.K. 2011. *Transport properties of high volume fly ash roller compacted concrete*. Cem. Concr. Compos, 33: 1057–1062.

BASSIST M., WĘGLEWSKI W. 2009. *Chemically assisted damage of concrete: a model of expansion under external sulfate attack*. Int. J. Damage Mech., 18(2): 155–175.

BENSTED J. 2000. *Fly ash of resistance to thaumasite sulphate attack*. CWB, 1: 14–16.

BENTZ D., FERRARIS C. 2010. *Rheology and setting of high volume fly ash mixtures*. Cem. Concr. Compos, 32: 265–270.

CHALEE W., TEEKAVANIT M., KIATTIKOMOL K., SIRIPANICHGORN A., JATURAPITAKKUL C. 2007. *Effect of W/C ratio on covering depth of fly ash concrete in marine environment*. Construction and Building Materials, 21: 965–971.

GARCIA-LODEIRO I., FERNANDEZ-JIMENEZ A., PALOMO A. 2013. *Variation in hybrid cements over time. Alkaline activation of fly ash-portland cement blends*. Cem. Concr. Res., 52: 112–122.

Environment protection. 2013. Główny Urząd Statystyczny (Central Statistical Office), p. 345, 346.

HA-WON S., CHANG-HONG L., KI YONG A. 2008. *Factors influencing chloride transport in concrete structures exposed to marine environments*. Cem. Concr. Compos, 30: 113–121.

KRUGER R. 2005. *Technologia przyszłości, perspektywy i przykłady. Popioły z energetyki*. Sopot, p. 9–20.

KURDOWSKI W. 2010. *Chemia cementu i betonu*. Stowarzyszenie Producentów Cementu, Kraków, Wydawnictwo Naukowe PWN, Warszawa.

LORENTE S., YSSORCHE-CUBAYNES M-P., AUGER J. 2011. *Sulfate transfer through concrete: Migration and diffusion results*. Cem Concr Compos, 33: 735–741.

LOTHENBACH B., BARY B., LE BESCOP P., SCHMIDT T., LETERRIER N. 2010. *Sulfate ingress in Portland cement*. Cem. Concr. Res., 40: 1211–1225.

MARCHAND J., SAMSON E., MALTAIS Y., BEAUDOIN J. 2002. *Theoretical analysis of the effect of weak sodium sulfate solutions on the durability of concrete*. Cem. Concr. Compos, 24 (3–4): 317–329.

NEVILLE A. 2012. *Właściwości betonu*. V edition. Stowarzyszenie Producentów Cementu, Kraków.

RUDZIŃSKI A. 2013. *Optymalizacja składu i trwałość kompozytów cementowo-popiołowych z dodatkiem włókien stalowych poddanych korozji*. Marine Engineering and Geotechnology, 5: 416–421.

SAHMARAN M., KASAP O., DURU K., YAMAN I. 2007. *Effects of mix composition and water-cement ratio on the sulfate resistance of blended cements*. Cem. Concr. Compos, 29: 159–67.

SANTHANAM M., COHEN M., OLEK J. 2006. *Differentiating seawater and groundwater sulfate attack in Portland cement mortars*. Cem. Concr. Res., 40: 1211–25.

SCHMIDT T., LOTHENBACH B., ROMER M., NEUENSCHWANDER J., SCRIVENER K. 2012. *Physical and microstructural aspects of sulfate attack on ordinary and limestone blended Portland cements*. Cem. Concr. Res., 39 (12): 1111–1121.

SPIESZ P., BROUWERS H. 2013. *The apparent and effective chloride migration coefficients obtained in migration tests*. Cem Concr Res., 48: 116–127.

SVOBODA M., LADERÉROVA J., SUCHARDOVA M., LEBER P. 2007. *Use of products of coal combustion in the construction industry and related industries in connection with the European regulation REACH*. Conference: Ashes from the power industry, p. 151–162.

TKACZEWSKA E., MAŁOLEPSZY J. 2009. *Effect of the fly ash fineness on the sulphate resistance of fly ash cement*. CWB, 1: 26–33.

Technical Sciences 17(4), 2014, 371–379

CHANGES IN MAGNETIC DOMAIN STRUCTURE OF MARAGING STEEL STUDIED BY MAGNETIC FORCE MICROSCOPY

Mirosław Bramowicz[1], *Sławomir Kulesza*[2], *Grzegorz Mrozek*[1]

[1] Chair of Materials and Machinery Technology
[2] Chair of Relativistic Physics
University of Warmia and Mazury in Olsztyn

Received 29 September 2014, accepted 19 November 2014, available on line 24 November 2014.

K e y w o r d s: Maraging Steel, Magnetic Force Microscopy, Fractal Analysis.

A b s t r a c t

The paper presents results on whether and how the magnetic domain structure in maraging steel undergoes any change due to the aging process. It continues the works on application of correlation methods and fractal analysis into studies of magnetic properties of various steel alloys using Scanning Probe Microscopy. It is aimed at verifying the usefulness of the structure function for description of spatial changes in shape and orientation of magnetic domains, and the magnitude of magnetic stray field affected by the heat treatment.

Obtained results suggest that despite vanishing magnetic tip-surface interaction, and hence vanishing magnetic stray field, magnetic domains remain nearly perfectly isotropic although randomly oriented. Similar to isotropic real surfaces, the fractal dimension of the magnetic domains turns out to be independent of the structural changes induced by the aging process, whereas the topothesy is found to vary within order of magnitude along with changes in the magnetic stray field. After all, obtained results lead to conclusion that the aging process leaves its fingerprints in the structure of the steel alloys, which can be studied using numerical analysis of images of magnetic interactions between vibrating tip and the stray field.

Introduction

In the seventies, precipitation hardening steels gained large attention as attractive construction materials renowned for their advantageous properties, for example: high mechanical strength (up to 2.5 GPa), good plasticity, low susceptibility to cracking, and others (BOJARSKI, MATYJA 1983, DOBRZAŃSKI 2002). Having good mechanical properties, these steels were initially used in

Correspondence: Mirosław Bramowicz, Katedra Technologii Materiałów i Maszyn, Uniwersytet Warmińsko-Mazurski, ul. Oczapowskiego 11, 10-719 Olsztyn, phone: 48 89 523 38 55, e-mail: miroslaw.bramowicz@uwm.edu.pl

the aerospace, aviation as well as military industries, but then they were also recognized good tool materials. Among them, H15K20M3JPr (X2CoCrMoAl20-15-3 according to PN-EN 10027-1) steel was distinguished as it possessed not only high mechanical strength, and impact toughness (Rm = 1.2 GPa, KCU = 90 J/cm^2 after aging procedure), but also significant corrosion resistance. Although in the second half of the eighties, due to scarce natural resources, and high price of cobalt, it was partly replaced by several substitutes, but now it is becoming popular again as a material investigated in fundamental research using modern scientific methods and instruments.

This paper continues the works on application of correlation methods to study magnetic properties of steels from Scanning Probe Microscope (SPM) images, which were presented previously (BRAMOWICZ, KULESZA 2013, BRAMOWICZ et al. 2014). It is aimed at verifying fractal nature of magnetic domains derived from SPM images using autocorrelation functions of the first and second orders. Recorded SPM signal reflects magnetic interaction between the field emitted from the surface, and the magnetized tip. As mentioned previously, this study is devoted to analysis of H15K20M3JPr (X2CoCrMoAl20-15-3) steel subjected to the aging process at various temperatures. Phase precipitates caused by the aging are expected to influence the spatial structure of magnetic domains, and hence the magnitude of the stray magnetic field. Observed changes are characterized using the following parameters: root mean square deviation of the phase shift between forced cantilever oscillation and the driving signal (Sq), fractal dimension (D_{ACF}), and the topothesy (K_{ACF}). The fractal parameters (D_{ACF}, and K_{ACF}) are determined using the algorithm described elsewhere (BRAMOWICZ et al. 2014). First of all, the 1-dimensional autocorrelation function $R(\tau)$ (ACF) is to be computed from the profiles of the magnetic interaction map $z(x)$ according to:

$$R(\tau)\ \langle (z(x) - \langle z(x)\rangle \cdot (z(\ +\ \tau) - \langle z(x)\rangle)\rangle \tag{1}$$

where:
τ – is the discrete spatial lag along the scan axis, whereas <...> denotes the mean value. Having the ACF, the structure function $S(\tau)$ (SF) can be calculated in the next step using the relation given by SAYLES and THOMAS (1978):

$$S(\tau)\ =\ 2 \cdot (Sq^2 - R(\tau)) \tag{2}$$

Figure 1 shows an exemplary graph of the structure function obtained in this way. Note the two characteristic parts of the $S(\tau)$ curve drawn in a log-log plot delimited by the so-called corner frequency τ_c, which establishes the minimum spatial lag between uncorrelated points on the map of magnetic

interactions. In the first range ($\tau << \tau_c$), the structure function obeys the power law given by:

$$S(\tau) \propto \tau^{2(2-D_{\mathrm{ACF}})} \tag{3}$$

In the second range ($\tau >> \tau_c$), the ACF asymptotically goes to zero, and hence the SF is approaching a constant value:

$$S(\tau) \approx 2 \cdot Sq^2 \tag{4}$$

On the whole, the SF curve can be described by the equation:

$$S(\tau) = K\tau^{2(2-D_{\mathrm{ACF}})} \tag{5}$$

where:
K – is the topothesy expressed according to WU (2002):

$$K = \frac{\pi G^{2(D_{\mathrm{ACF}}-1)}}{2\Gamma(5 - 2D_{\mathrm{ACF}} \sin[\pi(2 - D_{\mathrm{ACF}})]} \tag{6}$$

where:
Γ – is the Euler's gamma function.

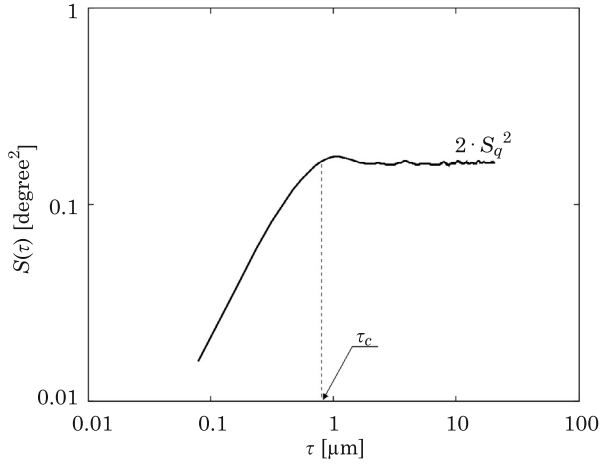

Fig. 1. Exemplary plot of the profile structure function

Experiment

Heat-treated samples of dimensions 25 × 45 × 5 mm were cut out of forged steel rod with a rectangular cross section of dimensions 100 mm by 100 mm. The heat treatment involved supersaturation at 1050°C for 30 min followed by recurrent aging cycles at increasing temperatures (500, 550, and 600°C, respectively). The aim of aging was to induce microstructural transitions within the steel responsible for changes in the magnetic domain structures, which were further studied using metallography, microhardness measurements, as well as Magnetic Force Microscopy (MFM), i.e. one of SPM modes.

Prior to metallographic examination, samples were polished, and etched in a Marble reagent. The measurements were carried out using Olympus XC-70 microscope with digital image acquisition. In turn, HV0.1 microhardness measurements were done using Innovatest 413D instrument in accordance with ISO 6507-1 standard. Magnetic domains were studied using Multimode 8 Scanning Probe Microscope (Bruker) with Nanoscope V controller (Bruker). In order to enhance the magnetic interaction, the scanning probes (MESP from Bruker, with 35 nm tip radius, and 400 Oe coercivity) were magnetized using strong permanent magnet prior to the measurements. The measurements were carried out in a two-pass mode, which was described in details elsewhere (BRAMOWICZ, KULESZA 2014), passing the scanning probe with the lift height 100 nm above the surface.

Results and discussion

Microstructural investigations of a sample in a supersaturated state reveal coarse microstructure of the alloy containing small non-metallic inclusions. This microstructure, together with microhardness as well as magnetic domain pattern, is significantly changed due to the aging. More specifically, the alloy initially exhibits coarse, polygonal structure of supersaturated austenite, but after the heat treatment at 500, 550 i 600°C, characteristic twins appear in its structure. The twins with small precipitates of intermetallic phases are located mostly in the austenite grain boundaries. It can be also seen coagulation of precipitated phases, which progressively increases with increasing aging temperature. Discussed changes in microstructure caused by the heat treatment are shown in Figure 2.

Precipitation of intermetallic phases from supersaturated solution significantly influences structural composition of the alloy, and hence its microhardness, as seen in Figure 3. On the other hand, microstructural changes in the

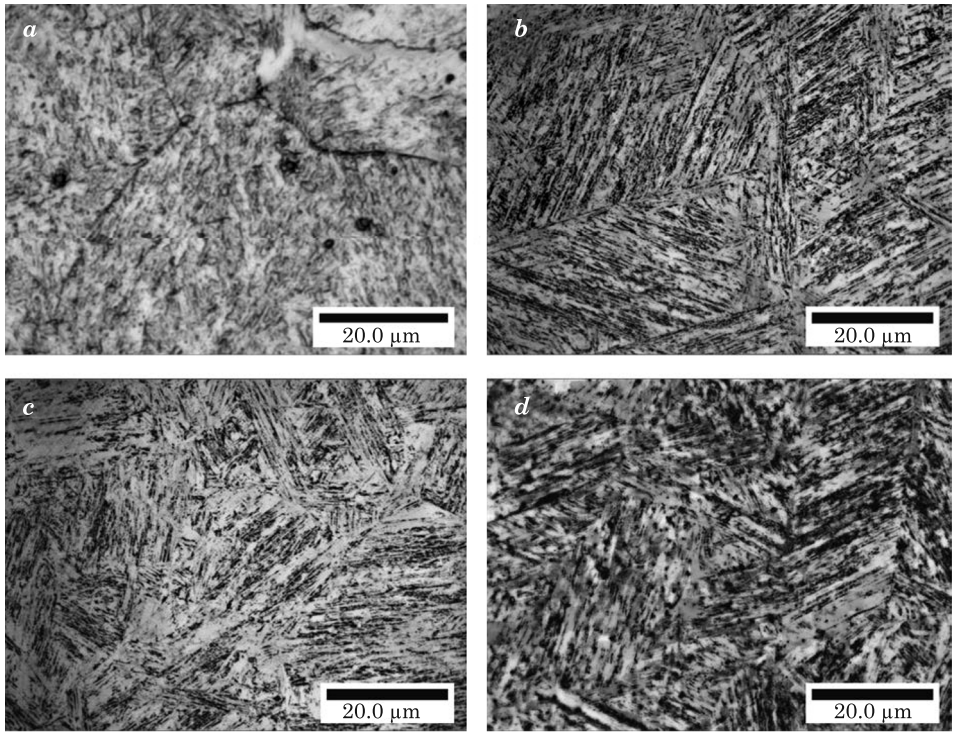

Fig. 2. Microstructure of X2CoCrMoAl20-15-3 steel in a supersaturated state (*a*), and after aging at, respectively: *b*) 500°C, *c*) 550°C, *d*) 600°C

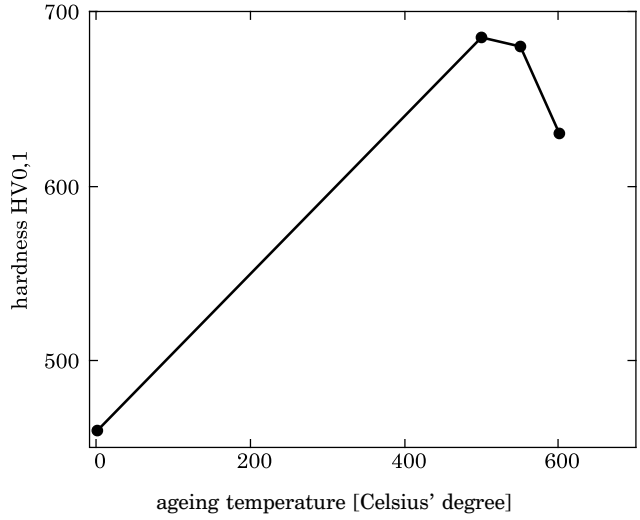

Fig. 3. Changes in microhardness due to the aging process

alloy's lattice are likely to modify the pattern of magnetic domains together with its characteristic parameters.

Figure 4 shows the images of magnetic stray field over the samples surface. Obtained results clearly indicate vanishing phase shifts between vibrating cantilever and the driving signal, which are due to decreasing tip-surface magnetic interaction. In addition, magnetic domains are becoming blurry pointing at discontinuities in magnetic material associated with precipitations of non-magnetic phases. The latter observation is supported by decreasing root-mean-square deviations of the phase shifts shown in Figure 5a.

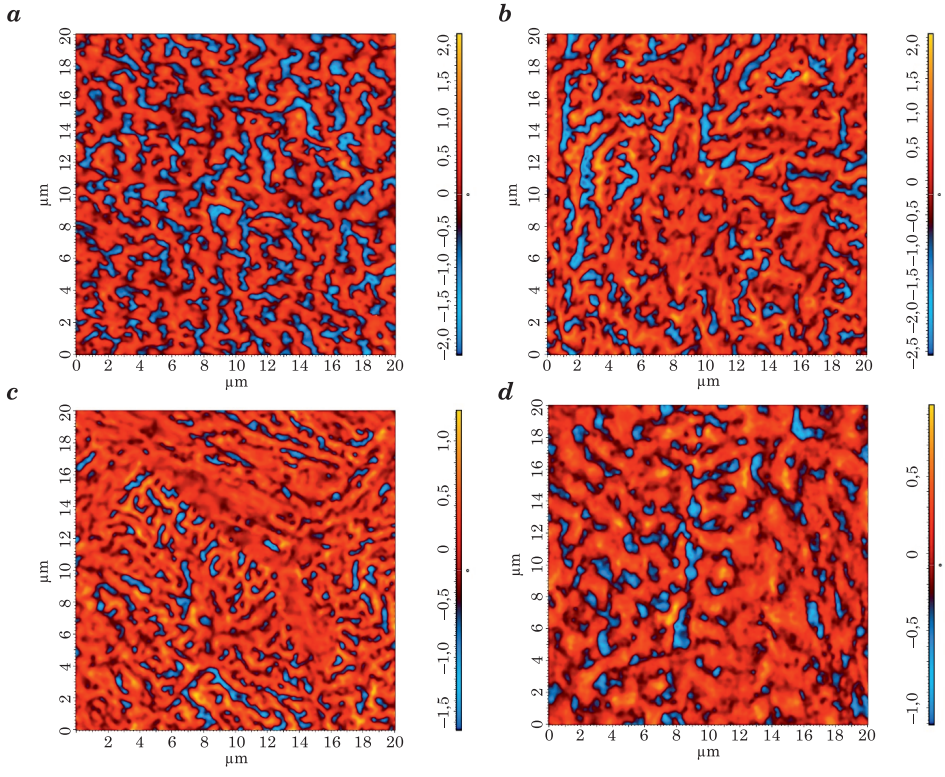

Fig. 4. Magnetic domains in X2CoCrMoAl20-15-3 steel in a supersaturated state (*a*), and after the aging at, respectively: *b*) 500°C, *c*) 550°C, *d*) 600°C

Figure 5b, and 5c show results of the fractal analysis that investigates self-affine properties of the magnetic domains. First of all, domains observed in Figure 4 exhibit random orientation, that is, they look nearly identical in all directions. In order to confirm this suggestion, the measure of anisotropicity is estimated, the so-called anisotropy ratio S_{tr}, according to method described elsewhere (BRAMOWICZ, KULESZA 2013). Basically, anisotropy ratio is defined

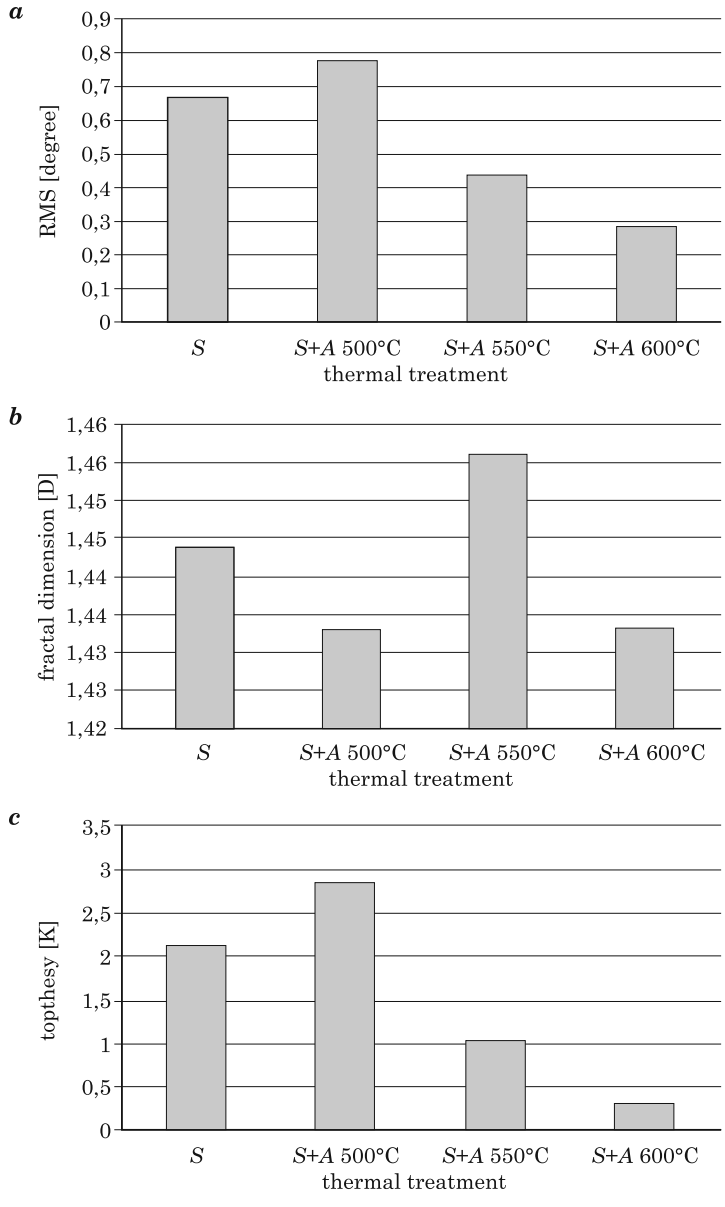

Fig. 5. Influence of the thermal treatment on: *a*) the phase shift between cantilever oscillations and the driving piezo signal (RMS values), *b*) fractal dimension *D*ACF, *c*) topothesy K

as a ratio between minimum and maximum autocorrelation decay lengths, along which the autocorrelation function decreases from $R = 1.0$ down to $R = 0.2$ (MAINSAH et al. 2001):

$$0 < S_{tr} = \frac{\tau_{\min}}{\tau_{\max}}\Bigg|_{R=1\rightarrow 0.2} \leq 1 \tag{7}$$

where:
$\tau_{\min}$ and $\tau_{\max}$ – the lengths of the decay of the autocorrelation function from $R = 1.0$ down to 0.2 along main anisotropy directions a_1 and a_2, respectively. Anisotropy ratio computed for domain images in Figure 4 is found at, respectively: 0.86, 0.86, 0.84, and 0.84. After all, such S_{tr} values (close to 1.0) confirm high isotropicity, and almost no influence of the aging process on the domain orientation.

Similarly, Figure 5b shows that the heat-treatment also has insignificant influence on the fractal dimension D_{ACF} that varies in the range from 1.43 to 1.46, that is within 2 per cent. On the other hand, Figure 5c exhibits large changes in the topothesy due to the aging process, which falls in the range from 0.25 up to 3, i.e. varies within order of magnitude under the treatment. In general, these observations are in good agreement with previous findings on the fractal properties of real surfaces, according to which in isotropic specimens fractal dimension remains constant, but the topothesy is sensitive to structural changes.

Conclusions

The following conclusions can be drawn from performed measurements:

1. Fractal analysis together with fractal parameters are useful tools for mathematical description of evolution of magnetic domains in terms of their shape, orientation, and the magnitude of the magnetic stray field similar to surfaces of real 3-dimensional objects.

2. Changes in topothesy are proportional to those in magnetic tip-surface interaction.

3. Changes in magnetic tip-surface interaction have no influence on the fractal dimension D_{ACF} unless significant changes in the domains' structure occur.

References

BOJARSKI Z., MATYJA P. 1983. *Stale maraging – tworzywo narzędziowe.* Prace naukowe Uniwersytetu Śląskiego w Katowicach, 589.

BRAMOWICZ M., KULESZA S., CZAJA P., MAZIARZ W. 2014. *Application of the autocorrelation function and fractal geometry methods for analysis of MFM images*. Archives of Metallurgy and Materials, 59(2): 441–457.

BRAMOWICZ M., KULESZA S. 2013. *A Magnetic Force Microscopy Study of Magnetic Domain Structure in Maraging Steel*. Solid State Phenomena, 203–204: 315–318.

DOBRZAŃSKI L.A. 2002. *Podstawy nauki o materiałach i metaloznawstwo*. Wydawnictwo Naukowo-Techniczne, Warszawa.

MAINSAH E., GREENWOOD J.A., CHETWYND D.G. 2001. *Metrology and Properties of Engineering Surfaces*. Kluwer Academic Publishers.

SAYLES R., THOMAS T.R. 1978. *Surface topography as a non-stationary random process.* Nature, 271: 431–434.

WU J.J. 2002. *Analyses and simulation of anisotropic fractal surfaces*. Chaos, Solitons and Fractals, 13: 1791–1806.

Technical Sciences 17(4), 2014, 381–390

RESEARCH AND MODELING OF PROCESSES IN THE FLUIDIZED BED OPPOSED JET MILL

***Henryk Otwinowski*[1], *Vladimir Pavlovich Zhukov*[2], *Tomasz Wyleciał*[3], *Anton Nikolaevich Belyakov*[2], *Aleksandra Górecka-Zbrońska*[1]**

[1] Institute of Thermal Machinery
Częstochowa University of Technology
[2] Department of Applied Mathematics
Ivanovo State Power University, Russia
[3] Department of Industrial Furnaces and Environmental Protection
Częstochowa University of Technology

Received 5 October 2014, accepted 7 November 2014, available on line 11 November 2014.

Key words: fluidized bed opposed jet mill, grinding, classification, matrix model, selection function, cut size, Tromp curve.

Abstract

A model of the grinding and classification processes in the fluidized bed opposed jet mill based on the Markov chains approach was proposed. The methodology of modelling was elaborated and experimental research of the combined processes of grinding and classification was carried out.

Introduction

Currently, the fluidized bed opposed jet mills are widely used in many industries for preparation of pure fine powders (OGURTZOV et al. 2004, p. 122–124,). Many publications are devoted to the studies of the grinding process in these mills (PALANIANDY et al. 2008, p. 380–388, FUKUNAKA et al. 2006, p. 89–96, BERTHIAUX, DODDS 1999, p. 78–87, MIZONOV et al. 1997), while the process of classification in the mills is rarely discussed. Description of classification of granular materials in the operating volume of such mills is rather complicated because several processes go simultaneously. In this paper the methodology of decomposition of the total process in a fluidized bed opposed jet

Correspondence: Henryk Otwinowski, Instytut Maszyn Cieplnych, Politechnika Częstochowska, al. Armii Krajowej 21, 42-201 Czestochowa, phone: 48 34 3250 579, e-mail: otwinowski@imc.pcz.czest.pl

mill is proposed as well as a model of each sub-process inside it. Description of separated processes and their synthesis was carried out with the use of the theory of Markov chains, which is often used to model various processes in powder technology (BERTHIAUX et al. 2005, p. 128–137, MIZONOV et al. 2008, p. 335-340, OTWINOWSKI 2014, p. 399–403).

Experimental set-up

The investigation of comminution was carried out at the experimental set-up schematically presented in Figure1. A laboratory fluidized bed opposed jet mill, which is designed for fine grinding of granular materials, is the basic element of the set-up. The experimental set-up was equipped with the following systems ensuring the correct work of the mill:

– the material feed system to the mill (charging container, conveyer),

– the air feed system to the mill (compressor, pressure fan, vacuum cleaner),

– the separation system of fine product and the system of cleaning the coming out air (flow classifier, separation cyclone and cloth filter).

The working air is supplied to the mill by the compressor 1 and the sealing air is supplied by the vacuum cleaner 13. The granular feed material with known particle size distribution is fed to the cylindrical milling chamber 6 gravitationally from the charging container 8. The feed material undergoes an extensive fluidization by means of the air jets from the nozzles 5. The nozzles inject air concentrically with the controlled flow rate $\dot{V}$ and overpressure p with thw flow velocity u. The mass flow rate of working air is measured by the rotameter 2, while the overpressure – by the elastic pressure gauge 4. Symmetrical design of the air collector 3 ensures homogeneous air distribution over individual jets and its dehydration and de-oiling. The collision of opposed air jets and turbulent fluidization state in the grinding chamber makes it possible to obtain a high-energy fluidization layer. This layer, in turn, ensures effective grinding of granular material. The rotor classifier 7 is installed above the grinding chamber 6 in the range of fountain flow of ground particles. The classifier separates the ground material into the fine fraction directed to the cyclone 9 and the coarse fraction directed to the milling chamber for repeated grinding. The cut size of classification can be controlled by regulation of angular speed of the rotor. The classifier makes it possible to obtain very fine milling product without the so-called mesh fraction (presence of coarse particles in a fine-ground product). Separation of the fine particles from the air after classification occurs in the cyclone 9. The air-particle mixture is separated into the flow dusted working air that is directed to the cloth filter 11 and

the flow of milling product I that is directed to the container 10. The solid particles in air, which was not captured in the cyclone, are captured in the cloth filter. These particles as the milling product II together with milling product I are the total product of fluidized-jet grinding. A negative pressure is assured by a vacuum cleaner 12.

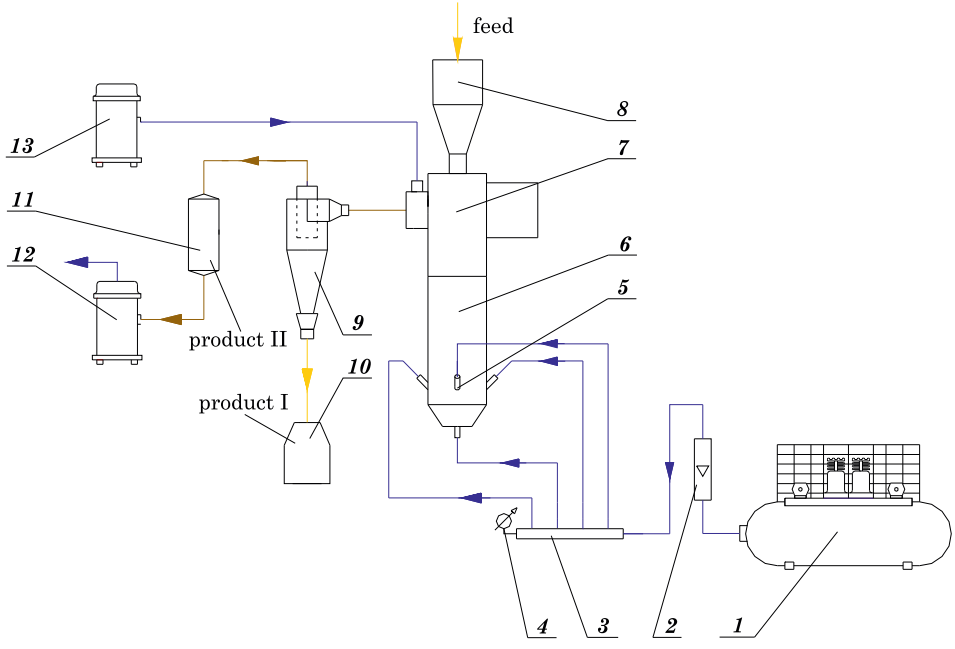

1 – compressor, *2* – rotameter, *3* – collector of working air, *4* – elastic pressure gauge, *5* – air nozzles, *6* – grinding chamber, *7* – rotational flow classifier with electric motor, *8* – filling container of feed material, *9* – cyclone, *10* – container of milling product I, *11* – cloth filter (milling product II), *12* – vacuum cleaner of exhaust air, *13* – vacuum cleaner of seal air

Fig. 1. Schematic diagram of the experimental set-up

Modeling and identification of processes in the fluidized bed opposed jet mill

The grinding of material in the fluidized bed opposed jet mill is primarily due to abrasion of the grains. During the grinding the fine particles detached from the feed particles. After grinding, the feed particles pass into two classes: fine and the neighboring to the feed one. On the basis of the mass balance of the particles population the grinding process can be described by the following matrix equation (BERTHIAUX et al. 2005, p. 128–137):

$$\mathbf{F}^{k+1} = \mathbf{G}\,\mathbf{F}^{k} \tag{1}$$

where:
F – the particle size distribution of the material expressed by the column vector,
G – the grinding matrix,
k is the discrete time of the process (the number of time transition).

The discrete time step of the process is equal to:

$$k = \frac{t}{\Delta t} \tag{2}$$

where:
t – the total duration of experiment of the batch grinding,
Δt – the dimensional time step.

The matrix **G** of grinding has the following form:

$$\mathbf{G} = \begin{bmatrix} g_{11} & 0 & \ldots & 0 & 0 \\ g_{21} & g_{22} & \ldots & 0 & 0 \\ 0 & g_{32} & \ldots & 0 & 0 \\ \ldots & \ldots & \ldots & \ldots & \ldots \\ 0 & 0 & \ldots & g_{m-1m-1} & 0 \\ g_{m1} & g_{m2} & \cdots & g_{mm-1} & g_{mm} \end{bmatrix} \tag{3}$$

where:
g_{ij} – the part of the fraction j that transits into the fraction i during Δt due to grinding, m – the total number of fractions under observation.

The probability of particles transition from class j to class i as a result of grinding during Δt can be determined from the following relationship:

$$g_{ij} = \begin{cases} 1 - S_j \Delta t, & i = j \\ \dfrac{S_j x^{v}_{j+1}}{x^{v}_{j+1} + x^{v}_{m}}\,\Delta t, & i = j + 1 \\ \dfrac{S_j x^{v}_{m}}{x^{v}_{j+1} + x^{v}_{m}}\,\Delta t, & i = m \\ 0, & i \neq j, j + 1, m \end{cases} \tag{4}$$

where:
S – the selection function,
ν – the particle shape parameter and $\nu = 1$ for needle particles, $\nu = 2$ for flat particles, $\nu = 3$ for the three-dimensional particles.

It is assumed that the selection function has the exponential form

$$S_j = \alpha x_j^r \tag{5}$$

where:
α and r are the constant coefficients (identification parameters).

The experimental identification of the grinding model was performed with the described above laboratory set-up for three durations of the grinding test: 20, 40 and 60 minutes. Samples of limestone with the particles size range 0–2 mm from „Czatkowice" Mine in Krzeszowice near Cracow were used in the tests. Milling product I (from the cyclone) and milling product II (from the filter) were mixed to represent the ground material. Then representative samples of the feed and total ground product were taken to determine the particle size distribution with the use of the Infrared Particle Sizer (IPS) analyser manufactured by Kamika Instruments. The results are shown in Figure 2.

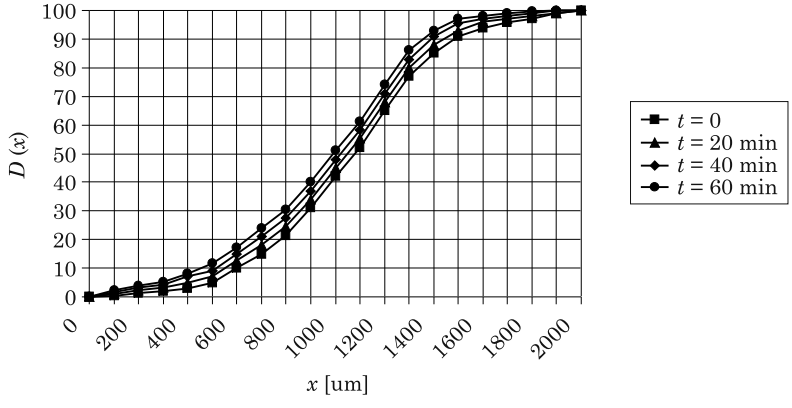

Fig.2. Particle size distribution in the feed ($t = 0$) and total ground product after various durations of grinding test

Particle size distribution in the ground product depends significantly on the material mass in the fluidized bed. In order to determine the dependence of the parameter α on the mass of the material in the bed the series of

experimental tests for various value of the mass in the range 0.5–3.5 kg were performed. Theoretical analysis of the test results allowed obtaining the following correlation:

$$\alpha = 0.0116 + 0.0084 \cdot M - 0.0021 \cdot M^2 \tag{6}$$

Figure 3 shows comparison of experimental and computational data for the cumulative undersize distribution D_j (points correspond to various particle size x_j). The comparison looks rather satisfactory excepting small deviation in the range of very fine particles.

It is interesting to note that, due to Eq. (6), there exists the optimum value of the hold-up (M = 2 kg) that corresponds to the maximum rate of grinding. The following explanation of the fact can be suggested. At small hold-up the air jets penetrate deeply into the bed and transfer to particles high kinetic energy but because of small particle concentration the probability of inter-particle collision is small and the rate of grinding is small. On the opposite, at high hold-up this probability is high but the depth of jets penetration is small and particle kinetic energy is small. It leads to the optimum hold-up at which these opposite tendencies are combined in the rational way.

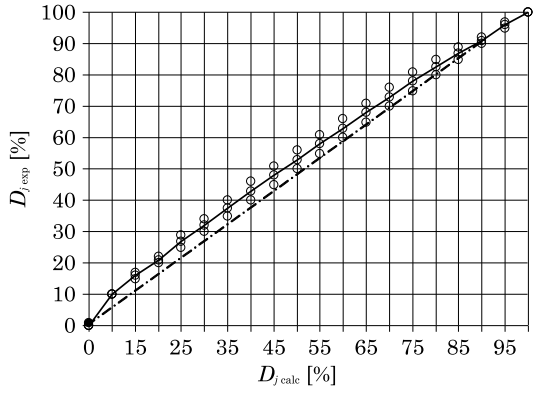

Fig. 3. Comparison of experimental and calculated data according to the proposed grinding model

In modeling the classification process two stages of it were taken into consideration: the gravitational stage and centrifugal stage. In the two-stage classifier the feed material to the classifier is separated into two products: fine and coarse-ground. A commonly used characteristic of such classifier is the Tromp curve $C(x)$, which shows the part of a fraction that goes to the fine product as a function of the fraction size. The discrete analogue of the Tromp curve is the matrix of classification **C**:

$$\mathbf{C} = \begin{bmatrix} c_{11} & 0 & 0 & \ldots & 0 \\ 0 & c_{22} & 0 & \ldots & 0 \\ 0 & 0 & c_{33} & \ldots & 0 \\ \ldots & \ldots & \ldots & \ldots & \ldots \\ 0 & 0 & 0 & \ldots & c_{mm} \end{bmatrix} \tag{7}$$

Very often the Molerus's formula is used to describe the Tromp curve (MIZONOV et al. 1997):

$$C(x_j) = \frac{1}{1 + \exp(E[x_j/x_c)^2 - 1\ ])} \tag{8}$$

where:

E – the particle separation efficiency parameter to be determined experimentally,
x_c – the cut size, for which the particle has the equal probability 0.5 to appear in the both products.

Particle size distribution in the fine product $\mathbf{F}_3$ and in the coarse product $\mathbf{F}_2$ of classification can be calculated from the following equations (MIZONOV et al. 1997):

$$\begin{aligned} \mathbf{F}_3 &= \mathbf{C}\mathbf{F}_1 \\ \mathbf{F}_2 &= (\mathbf{I} - \mathbf{C})\mathbf{F}_1 \end{aligned} \tag{9}$$

where:
$\mathbf{F}_1$ – the particle size distribution in the feed material,
$\mathbf{I}$ – the identity matrix.

The particle size distributions $\mathbf{F}_3$ and $\mathbf{F}_2$ are normalized to the unit mass portion of the feed.

The complex nature of particles motion in the fluidized bed makes the study of classification process difficult. Due to the fact that the processes of grinding and classification go simultaneously in order to study pure classification in the mill the quartz sand was used in these experiments, which is practically not being ground in the grinding zone. The specificity of the experimental identification of the classification model is that the process takes place in the two stages of classification simultaneously. The efficiency of the gravitational stage strongly depends on the air flow rate through the milling chamber and on the hold-up. The centrifugal stage mainly depends on the

rotor speed and air flow rate. Identification of the gravitational stage was based on experimental results for the grinding chamber without the centrifugal stage (at zero angular speed of the classifier rotor). During the study the following process parameters were measured in the experiments: the atmospheric pressure p_a, the pressure of working air at the mill inlet p, the rotational speed of the classifier rotor n, the duration of the experiment τ, the mass of the feed material m_N, the mass of material in the chamber m_K, the mass of material from the cyclone m_c, the volumetric flow rate of air Q. The particle size distribution in the loose materials was measured with the electronic analyzer IPS Kamika Instruments. The particle size distribution in the fine product of the gravitational stage, determined for different values of the air flow rate, is the particle size distribution in the feed material to the centrifugal stage. The centrifugal classification process was tested for the angular speed of the rotor within the range 0–25 1/s.

Figure 4 shows the experimental dependence of the mass fraction of the coarse product of the centrifugal stage on the volumetric air flow rate at various values of rotational speed of the classifier rotor. The experimental results allowed determining the cut size for the gravitational and centrifugal stage. The procedure is based on the equations (9) with the use of the method of least squares. Theoretical foundations of modelling the multi-stage classification are described in the paper OTWINOWSKI (2014, p. 399–403). The results are shown in Figure 5.

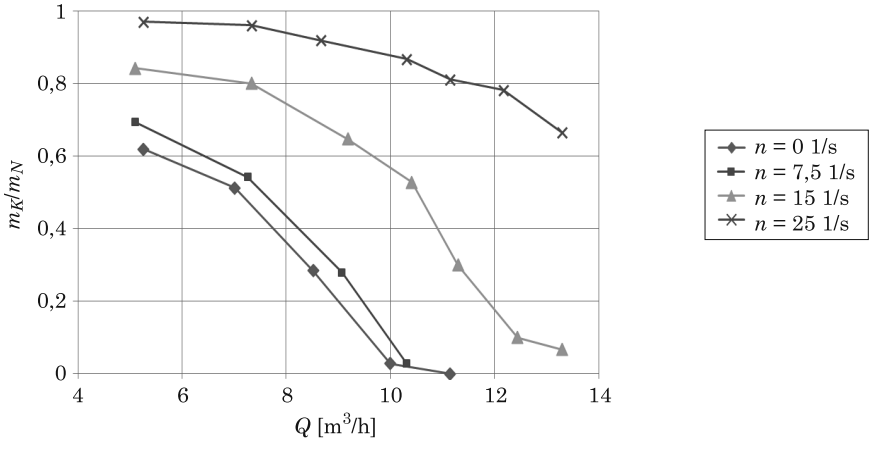

Fig. 4. Influence of the air flow rate Q on the mass fraction of coarse product at different angular speed of the classifier rotor

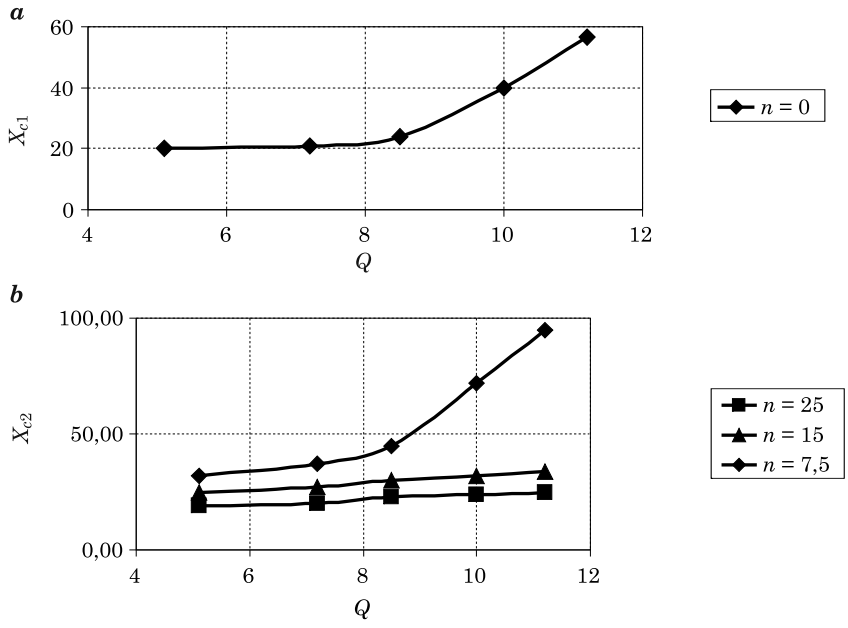

Fig. 5. Particle cut size of the gravitational and centrifugal classification as the function of the air flow rate Q [m^3/h] at different rotational speed n [1/s] of the classifier rotor

Summary

The proposed models of grinding and classification of granular material in the opposed fluidized bed jet mill makes it possible to describe the particle size distribution after any stage of the combined process grinding plus classification. Results of numerical experiments with the model can be used in the design and optimization of equipment for grinding and classification.

References

OGURTZOV A.V., ZBRONSKI D., ZHUKOV V.P., OTWINOWSKI H., URBANIAK D. 2004. *Method of calculation of fluidized bed opposed jet mill*. Chemistry and Chemical Technology, 10: 122–124.

PALANIANDY S., AZIZLI K., HUSSIN H., HASHIM S. 2008. *Effect of operational parameters on the breakage mechanism of silica in a jet mill*. Minerals Engineering, 21: 380–388.

FUKUNAKA T., GOLMAN B., SHINOHARA K. 2006. *Batch grinding kinetics of Ethenzamide particles by fluidized-bed jet-milling*. International Journal of Pharmaceutics, 311: 89–96.

BERTHIAUX H., DODDS J. 1999. *Modeling fine grinding in a fluidized bed opposed jet mill*. Part I. *Batch grinding kinetics*. Powder Technology, 106: 78–87.

MIZONOV V., ZHUKOV V., BERNOTAT S. 1997. *Simulation of grinding: new approaches*. ISPEU Press, Ivanovo.

BERTHIAUX H., MIZONOV V., ZHUKOV V. 2005. *Application of the theory of Markov chains to model different processes in particle technology*. Powder Technology, 157: 128–137.

MIZONOV V., BERTHIAUX H., ARLABOSSE P., DJERROUD D. 2008. *Application of the theory of Markov chains to model heat and mass transfer between stochastically moving particulate and gas flows.* Granular Matter, 10: 335–340.

OTWINOWSKI H. 2014. *Modeling the multi-stage classification in a fluidized bed jet mill*. Particulate Science and Technology, 32(4): 399–403.

Technical Sciences
Reviewers of Years – book 2014

Cengiz Akdeniz
Daniel Alomar
Dariusz Asendrych
Mindaugas Augonis
Robertas Balevičius
Jani Barle
Ireneusz Białobrzewski
Davide Ciucci
James Cooper
Yalçyn Coşkuner
Ryszard Coufal
Daniel Cozzolino
William Craig
Dinara Dallaeva
Przemysław Drożyner
Guillermo Emilio Defosse
Vilis Dubrovskis
Stanisław Duer
Ramazan Cuneyt Erenoğlu
Józef Flizikowski
Glen Fox
Tomasz Goetzendorf-Grabowski
Leonel Francisco Castañeda Heredia
Peter Aba Idah
Rimantas Kačianauskas
Dong-Soo Kim
Krzysztof Klempka
Iwona Konopka
Aleksander Korjakins
Piotr Korzeniowski
Juraj Kralik
Magdalena Lahodová
Krzysztof Lipiński
Fan Min
Vadim Evgen'evich Mizonov
Matthias Moeller
Beatriz Molinuevo Salces
Wojciech Mueller
Ryszard Myhan
Arnoldas Norkus
Eimuntas Kazimieras Paršeliūnas
Atynç Pirti
Karel Rastočný
Martina Sacher
Stepan Savchuk
Ahmet Sıvacyoğlu
Wojciech Sobieski
Michael C. Sukop
Ziemowit Suligowski
Jacek Szumbarski
Zbigniew Ślipek
Dariusz Tomkiewicz
Koen Trouw
Szymon Wajda
Janusz Walo
Joanna Wiącek
Dorota Witrowa-Rajchert
Leo van Rijn
Eva Zdravecká
Milan Zmindak

Guide for Autors

Introduction

Technical Sciences is a peer-reviewed research Journal published in English by the Publishing House of the University of Warmia and Mazury in Olsztyn (Poland). Journal is published continually since 1998. Until 2010 Journal was published as a yearbook, in 2011 and 2012 it was published semiyearly. From 2013, the Journal is published quarterly in the spring, summer, fall, and winter.

The Journal covers basic and applied researches in the field of engineering and the physical sciences that represent advances in understanding or modeling of the performance of technical and/or biological systems. The Journal covers most branches of engineering science including biosystems engineering, civil engineering, environmental engineering, food engineering, geodesy and cartography, information technology, mechanical engineering, materials science, production engineering etc.

Papers may report the results of experiments, theoretical analyses, design of machines and mechanization systems, processes or processing methods, new materials, new measurements methods or new ideas in information technology.

The submitted manuscripts should have clear science content in methodology, results and discussion. Appropriate scientific and statistically sound experimental designs must be included in methodology and statistics must be employed in analyzing data to discuss the impact of test variables. Moreover there should be clear evidence provided on how the given results advance the area of engineering science. Mere confirmation of existing published data is not acceptable. Manuscripts should present results of completed works.

There are three types of papers: a) research papers (full length articles); b) short communications; c) review papers.

The Journal is published in the printed and electronic version. The electronic version is published on the website ahead of printed version of Technical Sciences.

Technical Sciences does not charge submission or page fees.

Types of paper

The following articles are accepted for publication:

Reviews

Reviews should present a focused aspect on a topic of current interest in the area of biosystems engineering, civil engineering, environmental engineering, food engineering, geodesy and cartography, information technology, mechanical engineering, materials science, production engineering etc. They should include all major findings and bring together reports from a number of sources. These critical reviews should draw out comparisons and conflicts between work, and provide an overview of the 'state of the art'. They should give objective assessments of the topic by citing relevant published work, and not merely present the opinions of individual authors or summarize only work carried out by the authors or by those with whom the authors agree. Undue speculations should also be avoided. Reviews generally should not exceed 6,000 words.

Research Papers

Research Papers are reports of complete, scientifically sound, original research which contributes new knowledge to its field. Papers should not exceed 5,000 words, including figures and tables.

Short Communications

Short Communications are research papers constituting a concise description of a limited investigation. They should be completely documented, both by reference list, and description of the experimental procedures. Short Communications should not occupy more than 2,000 words, including figures and tables.

Letters to the Editor

Letters to the Editor should concern with issues raised by articles recently published in scientific journals or by recent developments in the engineering area.

Contact details for submission

The paper should be sent to the Editorial Office, as a Microsoft Word file, by e-mail: techsci@uwm.edu.pl

Referees

Author/authors should suggest, the names, addresses and e-mail addresses of at least three potential referees. The editor retains the sole right to decide whether or not the suggested reviewers are used.

Submission declaration

After final acceptance of the manuscript, the corresponding author should send to the Editorial Office the author's declaration. Submission of an article implies that the work has not been published previously (except in the form of an abstract or as part of a published lecture or academic thesis or as an electronic preprint), that it is not under consideration for publication elsewhere, that publication is approved by all authors and tacitly or explicitly by the responsible authorities where the work was carried out, and that, if accepted, it will not be published elsewhere in the same form, in English or in any other language.

To prevent cases of ghostwriting and guest authorship, the author/authors of manuscripts is/are obliged to: (i) disclose the input of each author to the text (specifying their affiliations and contributions, i.e. who is the author of the concept, assumptions, methods, protocol, etc. used during the preparation of the text); (ii) disclose information about the funding sources for the article, the contribution of research institutions, associations and other entities.

Language

Authors should prepare the full manuscript i.e. title, abstract and the main text in English (American or British usage is accepted). Polish version of the manuscript is not required.

The file type

Text should be prepared in a word processor and saved in doc or docx file (MS Office).

Article structure

Suggested structure of the manuscript is as follows:

Title
Authors and affiliations
Corresponding author
Abstract
Keywords
Introduction
Material and Methods
Results and Discussion

Conclusions
Acknowledgements (*optional*)
References
Tables
Figures

Subdivision – numbered sections

Text should be organized into clearly defined and numbered sections and subsections (optionally). Sections and subsections should be numbered as 1. 2. 3. then 1.1 1.2 1.3 (then 1.1.1, 1.1.2, ...). The abstract should not be included in numbering section. A brief heading may be given to any subsection. Each heading should appear on its own separate line. A single line should separate paragraphs. Indentation should be used in each paragraph.

Font guidelines are as follows:
– Title: 14 pt. Times New Roman, bold, centered, with caps
– Author names and affiliations:12 pt. Times New Roman, bold, centered, italic, two blank line above
– Abstract: 10 pt. Times New Roman, full justified, one and a half space. Abstract should begin with the word Abstract immediately following the title block with one blank line in between. The word Abstract: 10 pt. Times New Roman, centered, indentation should be used
– Section Headings: Not numbered, 12 pt. Times New Roman, bold, centered; one blank line above
– Section Sub-headings: Numbered, 12 pt. Times New Roman, bold, italic, centered; one blank line above
– Regular text: 12 pt. Times New Roman, one and a half space,full justified, indentation should be used in each paragraph

Title page information

The following information should be placed at the first page:

Title

Concise and informative. If possible, authors should not use abbreviations and formulae.

Authors and affiliations

Author/authors' names should be presented below the title. The authors' affiliation addresses (department or college; university or company; city, state and zip code, country) should be placed below the names. Authors with the same affiliation must be grouped together on the same line with affiliation information following in a single block. Authors should indicate all affiliations with a lower-case superscript letter immediately after the author's name and in front of the appropriate address.

Corresponding author

It should be clearly indicated who will handle correspondence at all stages of refereeing and publication, also post-publication process. The e-mail address should be provided (footer, first page). Contact details must be kept up to date by the corresponding author.

Abstract

The abstract should have up to 100-150 words in length. A concise abstract is required. The abstract should state briefly the aim of the research, the principal results

and major conclusions. Abstract must be able to stand alone. Only abbreviations firmly established in the field may be eligible. Non-standard or uncommon abbreviations should be avoided, but if essential they must be defined at their first mention in the abstract itself.

Keywords

Immediately after the abstract, author/authors should provide a maximum of 6 keywords avoiding general, plural terms and multiple concepts (avoid, for example, 'and', 'of'). Author/authors should be sparing with abbreviations: only abbreviations firmly established in the field may be eligible.

Abbreviations

Author/authors should define abbreviations that are not standard in this field. Abbreviations must be defined at their first mention there. Author/authors should ensure consistency of abbreviations throughout the article.

Units

All units used in the paper should be consistent with the SI system of measurement. If other units are mentioned, author/authors should give their equivalent in SI.

Introduction

Literature sources should be appropriately selected and cited. A literature review should discuss published information in a particular subject area. Introduction should identify, describe and analyze related research that has already been done and summarize the state of art in the topic area. Author/authors should state clearly the objectives of the work and provide an adequate background.

Material and Methods

Author/authors should provide sufficient details to allow the work to be reproduced by other researchers. Methods already published should be indicated by a reference. A theory should extend, not repeat, the background to the article already dealt within the Introduction and lay the foundation for further work. Calculations should represent a practical development from a theoretical basis.

Results and Discussion

Results should be clear and concise. Discussion should explore the significance of the results of the work, not repeat them. A combined Results and Discussion section is often appropriate.

Conclusions

The main conclusions of the study may be presented in a Conclusions section, which may stand alone or form a subsection of a Results and Discussion section.

Acknowledgements

Author/authors should include acknowledgements in a separate section at the end of the manuscript before the references. Author/authors should not include them on the title page, as a footnote to the title or otherwise. Individuals who provided help during the research study should be listed in this section.

Artwork
General points

– Make sure you use uniform lettering and sizing of your original artwork

– Embed the used fonts if the application provides that option
– Aim to use the following fonts in your illustrations: Arial, Courier, Times New Roman, Symbol
– Number equations, tables and figures according to their sequence in the text
– Size the illustrations close to the desired dimensions of the printed version

Formats

If your electronic artwork is created in a Microsoft Office application (Word, PowerPoint, Excel) then please supply 'as is' in the native document format

Regardless of the application used other than Microsoft Office, when your electronic artwork is finalized, please 'Save as' or convert the images to one of the following formats (note the resolution requirements given below):

EPS (or PDF): Vector drawings, embed all used fonts

JPEG: Color or grayscale photographs (halftones), keep to a minimum of 300 dpi

JPEG: Bitmapped (pure black & white pixels) line drawings, keep to a minimum of 1000 dpi or combinations bitmapped line/half-tone (color or grayscale), keep to a minimum of 500 dpi

Please **do not**:
– Supply files that are optimized for screen use (e.g., GIF, BMP, PICT, WPG); these typically have a low number of pixels and limited set of colors
– Supply files that are too low in resolution
– Submit graphics that are disproportionately large for the content

Color artwork

Author/authors should make sure that artwork files are in an acceptable format (JPEG, EPS PDF, or MS Office files) and with the correct resolution. If, together with manuscript, author/authors submit color figures then Technical Sciences will ensure that these figures will appear in color on the web as well as in the printed version at no additional charge.

Tables, figures, and equations

Tables, figures, and equations/formulae should be identified and numbered consecutively in accordance with their appearance in the text.

Equations/mathematical and physical formulae should be presented in the main text, while tables and figures should be presented at the end of file (after References section). Mathematical and physical formulae should be presented in the MS Word formula editor.

All types of figures can be black/white or color. Author/authors should ensure that each figure is numbered and has a caption. A caption should be placed below the figure. Figure must be able to stand alone (explanation of all symbols and abbreviations used in figure is required). Units must be always included. It is noted that figure and table numbering should be independent.

Tables should be numbered consecutively in accordance with their appearance in the text. Table caption should be placed above the table. Footnotes to tables should be placed below the table body and indicated with superscript lowercase letters. Vertical rules should be avoided. Author/authors should ensure that the data presented in tables do not duplicate results described in figures, diagrams, schemes, etc. Table must be able to stand alone (explanation of all symbols and abbreviations used in table is required). Units must be always included. As above, figure and table numbering should be independent.

References

References: All publications cited in the text should be presented in a list of references following the text of the manuscript. The manuscript should be carefully checked to ensure that the spelling of authors' names and dates of publications are exactly the same in the text as in the reference list. Authors should ensure that each reference cited in the text is also present in the reference list (and vice versa).

Citations may be made directly (or parenthetically). All citations in the text should refer to:

1. Single author

The author's name (without initials, with caps, unless there is ambiguity) and the year of publication should appear in the text

2. Two authors

Both authors' names (without initials, with caps) and the year of publication should appear in the text

3. Three or more authors

First author's name followed by et al. and the year of publication should appear in the text

Groups of references should be listed first alphabetically, then chronologically.

Examples:

"... have been reported recently (ALLAN, 1996a, 1996b, 1999; ALLAN and JONES, 1995).

KRAMER et al. (2000) have recently shown..."

The list of references should be arranged alphabetically by authors' names, then further sorted chronologically if necessary. More than once reference from the same author(s) in the same year must be identified by the letters "a", "b", "c" etc., placed after the year of publication.

References should be given in the following form:

KUMBHAR B.K., AGARVAL R.S., DAS K. 1981. *Thermal properties of fresh and frozen fish.* International Journal of Refrigeration, 4(3), 143–146.

MACHADO M.F., OLIVEIRA F.A.R., GEKAS V. 1997. *Modelling water uptake and soluble solids losses by puffed breakfast cereal immersed in water or milk*. In Proceedings of the Seventh International Congress on Engineering and Food, Brighton, UK.

NETER J., KUTNER M.H., NACHTSCHEIM C.J., WASSERMAN W. 1966. *Applied linear statistical models* (4th ed., pp. 1289–1293). Irwin, Chicago.

THOMSON F.M. 1984. *Storage of particulate solids*. In M. E. Fayed, L. Otten (Eds.), Handbook of Powder Science and Technology (pp. 365–463). Van Nostrand Reinhold, New York.

Citation of a reference as 'in press' implies that the item has been accepted for publication.

Note that the full names of Journals should appear in reference list.

Submission checklist

The following list will be useful during the final checking of an article prior to the submission. Before sending the manuscript to the Journal for review, author/authors should ensure that the following items are present:

– Text is prepared with a word processor and saved in DOC or DOCX file (MS Office). One author has been designated as the corresponding author with contact details: e-mail address

– Manuscript has been 'spell-checked' and 'grammar-checked'

– References are in the correct format for this Journal

– All references mentioned in the Reference list are cited in the text, and vice versa

– Author/authors does/do not supply files that are too low in resolution

– Author/authors does/do not submit graphics that are disproportionately large for the content